FOSSIL ENERGY

DOE/BC/14977-6
(DE95000187)

IMPROVED EFFICIENCY OF MISCIBLE CO_2 FLOODS AND ENHANCED PROSPECTS FOR CO_2 FLOODING HETEROGENEOUS RESERVOIRS

Annual Report for the Period
April 14, 1994 to April 13, 1995

By
R. Grigg
J. Heller
D. Schechter

September 1995

Performed Under Contract No. DE-FG22-94BC14977

New Mexico Institute of Mining and Technology
Socorro, New Mexico

Bartlesville Project Office
U. S. DEPARTMENT OF ENERGY
Bartlesville, Oklahoma

DISCLAIMER

This report was prepared as an account of work sponsored by an agency of the United States Government. Neither the United States Government nor any agency thereof, nor any of their employees, makes any warranty, expressed or implied, or assumes any legal liability or responsibility for the accuracy, completeness, or usefulness of any information, apparatus, product, or process disclosed, or represents that its use would not infringe privately owned rights. Reference herein to any specific commercial product, process, or service by trade name, trademark, manufacturer, or otherwise does not necessarily constitute or imply its endorsement, recommendation, or favoring by the United States Government or any agency thereof. The views and opinions of authors expressed herein do not necessarily state or reflect those of the United States Government.

This report has been reproduced directly from the best available copy.

Available to DOE and DOE contractors from the Office of Scientific and Technical Information, P.O. Box 62, Oak Ridge, TN 37831; prices available from (615) 576-8401.

Available to the public from the National Technical Information Service, U.S. Department of Commerce, 5285 Port Royal Rd., Springfield VA 22161

DOE/BC/14977-6
Distribution Category UC-122

Improved Efficiency of Miscible CO_2 Floods and Enhanced Prospects for CO_2 Flooding Heterogeneous Reservoirs

Annual Report for the Period
April 14, 1994 to April 13, 1995

By
R. Grigg
J. Heller
D. Schechter

September 1995

Work Performed Under Contract No. DE-FG22-94BC14977

Prepared for
U.S. Department of Energy
Assistant Secretary for Fossil Energy

Jerry Casteel, Project Manager
Bartlesville Project Office
P.O. Box 1398
Bartlesville, OK 74005

Prepared by
New Mexico Institute of Mining and Technology
Petroleum Recovery Research Center
Socorro, NM 87801

TABLE OF CONTENTS

TABLE OF CONTENTS iii

LIST OF TABLES iv

LIST OF FIGURES v

ABSTRACT vi

EXECUTIVE SUMMARY 1

INTRODUCTION 2
- BACKGROUND 2
- PROGRAM OBJECTIVES 2
- REPORT CONTENT 2

TASK 1 : CO_2-FOAMS FOR SELECTIVE MOBILITY REDUCTION 3
- INTRODUCTION 3
- PRELIMINARY LABORATORY WORK 4
- CONCLUSIONS 10
- REFERENCES 11

TASK 2: REDUCTION OF THE AMOUNT OF CO_2 REQUIRED IN CO_2 FLOODING 18
- INTRODUCTION 18
- BACKGROUND 18
- EXPERIMENTAL TESTS 18
- SIMULATION 21
- CONCLUSIONS 27
- REFERENCES 28

TASK 3: LOW IFT MECHANISMS WITH APPLICATIONS TO MISCIBLE FLOODING IN FRACTURED RESERVOIRS 36
- INTRODUCTION 36
- STATUS OF PENDANT DROP APPARATUS 36
- INVESTIGATION ON PARACHOR METHOD FOR IFT PREDICTION 37
- CONCLUSIONS 48
- COMPLEMENTARY RESEARCH AND FIELD APPLICATIONS 49
- REFERENCES 50

CONCLUDING REMARKS 70

ACKNOWLEDGMENTS 70

LIST OF TABLES

TASK 1

Table 1-1. Slopes determined by the regression of the mobility measurements 12

TASK 3

Table 3-1. Slopes of IFT vs $\Delta\rho$ data from Macleod 54
Table 3-2. Theoretical Values of the Critical Exponents 54
Table 3-3. Parachors of Petroleum Components 55
Table 3-4. Correlation Coefficients of Hydrocarbon Parachors 58
Table 3-5. Parachors of Oil Cuts 58
Table 3-6. Composition and Properties of Reservoir Fluids 59
Table 3-7. Comparison of IFT Predictions with Measured Data 60

LIST OF FIGURES

TASK 1

Fig. 1-1. Schematic of the mobility measurement experimental setup 13
Fig. 1-2. Effect of core position on the mobility measurements. 13
Fig. 1-3. Dependence of mobility on permeability 14
Fig. 1-4. Dependence of mobility on permeability 14
Fig. 1-5. Dependence of mobility on permeability 15
Fig. 1-6. Dependence of mobility on permeability 15
Fig. 1-7. Dependence of mobility on permeability 16
Fig. 1-8. Schematic diagram of the experimental apparatus (phase one) 16
Fig. 1-9. Schematic diagram of the experimental apparatus (phase two) 17

TASK 2

Fig. 2-1. CO_2 density vs temperature and pressure. 30
Fig. 2-2. Slim tube apparatus. 30
Fig. 2-3. Recovery vs pressure 31
Fig. 2-4. Effect of pressure on sweep efficiency 31
Fig. 2-5. C10/C16-CO_2 oil recovery 32
Fig. 2-6. Comparison of the compositions 32
Fig. 2-7. CO_2 -Spraberry Px diagram 33
Fig. 2-8. Effect of foam on oil rate 33
Fig. 2-9. CO_2 injection profile comparison at 263 days of simulation 34
Fig. 2-10. Effect of scaling parameter F on oil rate 34
Fig. 2-11. Effect of limiting gas saturation (SGLIM) on oil rate 35
Fig. 2-12. Comparison of oil rate to the CO_2 injection cycles in well 32032 35

TASK 3

Fig. 3-1. Pendant drop for nitrogen/water system 61
Fig. 3-2. Interfacial tension vs density difference measurements by Macleod 61
Fig. 3-3. Interfacial tension vs reduced temperature for methyl ether and CO_2 62
Fig. 3-4. Slope (γ in Eq. 6) distribution of IFT vs ($1-T/T_c$) plots for 57 pure components 62
Fig. 3-5. Density difference vs reduced temperature for iso-butyric acid/water 63
Fig. 3-6. Interfacial tension vs density difference for methane-propane mixtures 63
Fig. 3-7. Interfacial tension vs density difference for water/alcohol/oil systems 64
Fig. 3-8. Interfacial tension vs density difference for N_2/oil systems 64
Fig. 3-9. Interfacial tension vs density difference for oil/CO_2 systems 65
Fig. 3-10. Parachor vs molecular weight for 20 normal paraffins 65
Fig. 3-11. Parachor vs molecular weight for 69 hydrocarbons 66
Fig. 3-12. Parachor vs molecular weight for 83 hydrocarbons 66
Fig. 3-13. Parachor vs molecular weight for 90 hydrocarbons 67
Fig. 3-14. Parachor vs molecular weight for 122 hydrocarbons 67

Fig. 3-15. Parachor vs molecular weight for 136 hydrocarbons 68
Fig. 3-16. Measured and PREOS-predicted IFTs of system VI 68
Fig. 3-17. PREOS-predicted IFTs of CO_2/Spraberry separator oil 69
Fig. 3-18. PREOS-predicted IFTs of CO_2/Spraberry reservoir oil 69

ABSTRACT

The overall goal of this project is to improve the efficiency of miscible CO_2 floods and enhance the prospects for flooding heterogeneous reservoirs. This objective is being accomplished by extending experimental research in three task areas: 1) foams for selective mobility control in heterogeneous reservoirs, 2) reduction of the amount of CO_2 required in CO_2 floods, and 3) miscible CO_2 flooding in fractured reservoirs. This report provides results of the first year of the three-year project for each of the three task areas.

In the first task, we are investigating a desirable characteristic of CO_2-foam called Selective Mobility Reduction (SMR) that promises an improvement in displacement efficiency by reducing the effects of reservoir heterogeneity. We have continued laboratory measurements of the mobility in single cores. The scope of the tests also has been expanded by pumping the high-pressure CO_2-foam through two cores in series and measuring the pressure drop across each during the same test. This, along with a second experimental innovation using a withdrawal pump to maintain pressure, enables us to compare directly the mobilities of high and low permeability cores. The system has been used to extend our results, showing that a greater SMR effect takes place at low flow velocities rather than at high rates of flow. Additionally, we have made progress in several different experiments with composite cores in which high and low permeability regions are in capillary contact. Initial tests on one of these systems have been performed and are described in the report.

In the second task, we report our preliminary results on the phase behavior tests of a West Texas crude with CO_2. We also report our progress on the implementations of foam features and horizontal wellbore formulation into reservoir simulators. The progress of the development of a preprocessor program that can generate input parameters for phase-behavior simulations is also reported.

In the third task, we report our results of prediction of multicomponent, reservoir condition interfacial tension (IFT). We will provide a simple methodology that will allow the reader to calculate IFT of any crude oil/gas system. Our endeavor into IFT research was necessitated in order to properly model non-equilibrium gravity drainage, an important recovery mechanism during gas injection in vertically fractured reservoirs. Thus, the IFT research complements a Class III field demonstration to test low IFT gravity drainage in the naturally fractured Spraberry Trend in West Texas. The PRRC has teamed with Parker and Parsley, Midland, TX to work on a CO_2 pilot under the DOE PON program.

EXECUTIVE SUMMARY

In Task 1, we have progressed further in our studies of Selective Mobility Reduction (SMR), the property of CO_2-foam by which it can reduce the mobility by a greater fraction in higher than in lower permeability cores. This property promises to improve displacement efficiency in CO_2 floods by reducing the effects of reservoir heterogeneity. During the first year of the project, several positive results have been accomplished. These include the verification of a new and faster experimental system that allows us to measure the mobilities of two cores in the same test, discovered that a greater SMR effect occurs more often at low flow velocities than high, and completed design and initial testing of a parallel system in which high and low permeability regions are in continual capillary contact during foam flow.

In Task 2, we have completed CO_2 swelling and miscibility tests for one West Texas crude and eleven continuous phase equilibrium tests on a second West Texas crude. We have also started examining pressure effects on oil recovery in a reservoir core during CO_2 gas injection. Foam features have been incorporated into two simulators: MASTER (Miscible Applied Simulation Techniques for Energy Recovery), obtained from the Department of Energy, and UTCOMP, provided by the University of Texas at Austin. Validation tests have been performed to assess the foam features' sensitivity and adequacy. We have implemented horizontal wellbore formulation into the simulator MASTER. We have developed a preprocessor program that can generate input parameters for phase-behavior simulations.

In Task 3, we are investigating multiphase flow behavior in fractured reservoirs. To gain an understanding of the complicated distribution and flow behavior of oil, brine, and gas in the presence of vertical fractures, we have pursued both theoretical and experimental investigations into interfacial tension (IFT). IFT is particularly important when describing gas injection in naturally fractured reservoirs, thus we have embarked on a program to predict IFT accurately at reservoir conditions for any fluid combination.The first year of Task 3 was spent designing, building, and testing a pendant-drop apparatus for measurement of reservoir condition IFT. We also have developed a theoretically correct methodology for prediction of IFT for multicomponent gas/oil systems. We have found that our method predicts multicomponent IFT of known reservoir fluid IFT measurements better than the methods currently available in the literature. This work was necessary as a precursor to modelling low IFT gravity drainage in vertically fractured reservoirs. Many of the ideas and models developed will be incorporated into a DOE Class III PON field demonstration, which will test the economic feasibility of CO_2 injection in the naturally fractured Spraberry Trend Area.

INTRODUCTION

BACKGROUND

Because of the importance of CO_2 flooding to the future oil recovery potential in New Mexico, the Petroleum Recovery Research Center (PRRC) has maintained a vigorous experimental program in this area of research for the past fifteen years. This research has been supported by the Department of Energy (DOE), the State of New Mexico, and a consortium of oil companies. Based on encouraging results obtained in a project entitled "Improvement of CO_2 Flood Performance," the DOE awarded a grant to the PRRC in 1989 to transfer promising research on CO_2-foam to a field demonstration site. As part of the field demonstration test, the PRRC provided laboratory and research support for the design of the project entitled "Field Verification of CO_2-Foam," and continued to perform experimental work related to mechanisms involved in CO_2 flooding. The current project is a continuation of the prior work.

With large quantities of oil unrecoverable in fractured reservoirs, new concepts are being considered for these reservoirs that have the potential of recovering huge volumes of the remaining oil. These new concepts demonstrate the need for research into improvements for CO_2 flooding in heterogenous reservoirs so that domestic oil recovery from these reservoirs can be maximized and premature abandonment of potentially productive wells by EOR can be avoided.

New concepts are being investigated that could provide a more favorable response from the use of foam for achieving mobility control in CO_2 floods, the possibility of obtaining good oil recovery efficiency by using less CO_2 than is commonly practiced in field operations, and the advantage of gravity drainage and imbibition in CO_2 flooding vertically fractured reservoirs.

PROGRAM OBJECTIVES

The objective of this work consists of an experimental research effort aimed at improving the effectiveness of CO_2 flooding in heterogeneous reservoirs. The intent is to investigate new concepts that can be applied by field operators within the next two to five years. The proposed activities will consist of experimental research in three closely related areas: 1) further exploration of the applicability of selective mobility reduction (SMR) in the use of foam flooding, 2) the possibility of higher economic viability of floods at slightly reduced CO_2 injection pressures, and 3) taking advantage of gravitational forces during low IFT, CO_2 flooding in tight, vertically fractured reservoirs.

REPORT CONTENT

This report describes work performed during the first year of the project. Separate discussions and supporting material are provided for each of the three task areas.

TASK 1 : CO_2-FOAMS FOR SELECTIVE MOBILITY REDUCTION

INTRODUCTION

The goal of this task is to evaluate the usefulness of an unusual property of high-pressure CO_2-foams known as Selective Mobility Reduction (SMR) in field CO_2 projects. This very promising effect of using CO_2-foam for mobility control has been observed in our laboratory[1-4] and in some other laboratories[5]. For Darcy flow of ordinary fluids in rocks, the mobility is observed to be proportional to rock permeability. In laboratory experiments with CO_2-foams, on the other hand, mobility is not only reduced, but often by a greater fraction in high rather than in low permeability cores. This situation,where the mobility is less than proportional to core permeability and foam flow through higher permeability rocks is at a lower rate than would be expected for the given pressure gradient, is called Selective Mobility Reduction (SMR).

During the flow of ordinary, Darcian fluids through natural reservoir rock, the heterogeneities that exist in the rock are reflected in a non-uniform flow velocity field. Thus, any displacement front ordinarily becomes continually more non-uniform during flow through the reservoir. SMR offers the promise of markedly reducing this variability of flow rates, so that displacement by CO_2-foam could show significantly higher displacement efficiency. In a displacement with CO_2-foam that shows SMR, foams will flow at the same velocity in high and low permeability regions, preserving the uniformity of the flood front while propagating through rocks with non-uniform permeability. Presumably, this can reduce the effect of both vertical and horizontal rock heterogeneity, and as a consequence, the use of a CO_2-foam showing SMR could delay the breakthrough of CO_2 and lead to a higher displacement efficiency throughout heterogeneous reservoirs.

Unfortunately, while SMR of foam has been measured experimentally with some surfactants in a wide range of reservoir rock samples,[1,2] it has been observed not to occur with other surfactants.[2] Therefore, the first objective of our laboratory tests is to identify one or more surfactants that can dependably generate CO_2-foam that exhibits SMR, and to define the concentration range and other limitations to which they are subject. A second difficulty is that, although SMR has been observed to different extents in laboratory cores for CO_2-foams made with several surfactants, there is still a major question concerning its utility in a reservoir. This is because in the tests made up to now, the cores in which the mobility was measured were relatively homogeneous, and the average mobilities of the cores were measured by themselves. In a reservoir, high and low permeability sections are often in close proximity (and in capillary contact) with each other. Experimental observations to study the affect of capillary contact will require a change in testing methods.

Prior to attacking the latter tests, then, preliminary laboratory work was aimed at exploring the occurrence of SMR in various domains of surfactant type and concentration, flow rates, foam quality, and rock type. This work has taken place in the first year of the project and has involved several types of experiments and core geometries. The work is now complete and is described in the first part of this Annual Report. It has left us in a position from which we can perform direct experiments to measure SMR in composite rocks that simulate more closely the heterogeneity that

exists in reservoir rocks. With the newly-designed tests using a composite core, we will try to determine the effect of intimate contact between high and low permeability regions on the existence and field utility of SMR.

PRELIMINARY LABORATORY WORK

This work has taken place in two different reservoir-state environments, which are both located in the Kelly building on the New Mexico Tech campus. The first of these (the series 1 experiments) have been performed in our regular foam laboratory. The tests measure the mobility of small cores measuring 1.0 inch in length and 0.5 inch in diameter, that are preceded in the flow stream by 0.5 inch long cores used as foam generators. Addressing concerns about the effect of geometry on these tests, we have also instituted a second set of experiments (Series 2) being performed in a different laboratory at the PRRC and using different equipment and larger cores, and providing a test-bed for the composite-core tests. The first of the Series 2 experiments were again performed to check the apparatus and verify the existence of SMR in Berea rock. The two sets of experiments are discussed below.

Test Series 1

To screen surfactants for SMR potential, we modified our standard high-pressure mobility experiment to expedite the measurements of the mobility of CO_2-foam through rock samples with different permeability. Two coreholders were assembled in series in the flow path of the CO_2-foam such that the mobilities of foams in two cores of different permeability can be measured simultaneously during a single experiment. The validity of this design was examined by interchanging the positions of two cores in the flow system during the mobility measurement. Additional mobility measurements have been performed to examine the effect of surfactant type, concentration, rock type and flow rate on SMR of CO_2-foam. The results and discussion of these tests are presented below.

The first of two modifications was made to increase the speed and efficiency of the tests. This change consisted of the insertion of a second coreholder and rock sample in series with the foam generator and first core in the system, to transport the mixture of dense CO_2 and brine or surfactant solution. Therefore, the flow of the two fluids were the same (in the steady state) for the two cores, and the mobilities could be observed by recording the pressure drops across each.

The second change was replacing the needle valve that had been used for control of flow rate. For this purpose, we added an additional, backwards-running Ruska pump (with a floating piston ahead of it) in the downstream of the apparatus. Although the individual flow rate of the CO_2 and the brine (or surfactant solution) is controlled by separate injection pumps, the additional pump makes it possible to maintain constant the total volumetric flow rate of CO_2-foam or CO_2-brine during the experiment. Thus, the same flow rate of CO_2 mixtures through each core at steady state is assured and the mobilities in high and low permeability rock samples can be determined simultaneously. Both of these changes are shown in Fig. 1-1. Because the CO_2-aqueous mixture is corrosive, the rear portion of the floating piston contains distilled water to protect the inside barrel of the pump.

Two surfactants, Chaser CD1045 and CD1050, were used in the Series I tests. They were supplied by Chevron Chemical Company as 46.7 wt% active and 70 wt% active aqueous solutions, respectively. In different tests, two surfactant concentrations, 500 ppm (near or below the critical micelle concentration of each surfactant) and 1000 ppm (above each surfactant's CMC) were used to generate the foam. These concentrations are calculated on an active basis. Simultaneous injection of CO_2 and brine or CO_2 and surfactant was maintained at a volumetric ratio of 4 to 1 (or quality of 80%) while the total flow rates were varied from 7.5 cc/hr to 15 cc/hr (corresponding to Darcy velocities of 4.7 ft/day to 9.4 ft/day). All experiments were conducted at 101 °F and 2100 psig.

Core samples used in this study were cut from two types of quarried rocks, Berea sandstone and Baker dolomite, and from one "preserved state" carbonate reservoir rock. The core plug used as a foam generator is 0.5 inch in diameter and 0.5 inch in length while other core samples are 0.5 inch in diameter and 1.0 inch in length. The permeability of Berea sandstone varies from 130 md to 900 md whereas the permeability of Baker dolomite varies from 30 md to 110 md. The reservoir type of rock used here was supplied by the Phillips Petroleum Company as a piece of core slab which was retrieved from an observation well located at the East Vacuum Grayburg San Andres Unit Field. This core slab was originally wrapped and sealed at the well site and contained the original reservoir fluids. Using the PRRC scanning minipermeameter, we measured 286 permeabilities on one flat surface of this core slab, with a 0.05 inch square grid. From this measured permeability map, we found the permeabilities to vary from 0.1 md to 900 md on a small area of surface (15 inch square). The permeabilities are not uniformly distributed and mostly are below 70 md. By carefully locating the high and low permeability regions on this core slab, we were able to cut several core plugs (with permeabilities ranging from 50 to 500 md) for the tests.

Four experiments were first conducted to examine the effect of core position on the results of mobility measurements in the new two-core system. The first two experiments were conducted with the high permeability core positioned ahead of the low permeability core whereas the other two experiments were conducted the other way around. Baker dolomite and fired Berea sandstone were used in these tests with surfactant CD1050. In Fig. 1-2, the mobility values are plotted with respect to the core permeabilities. From the results, it is evident that whether the high or low permeability core is placed first in the flow stream is not significant. A line connecting the data points of different permeability indicates the relationship between mobility of fluid and the rock permeability. For an ordinary fluid flowing through different permeability rock samples, the mobilities are proportional to the rock's permeabilities, and the slope of the line should be 1.0. On the other hand, for a foam showing an ideal SMR (where the mobility of foam is roughly the same at high and low permeability), the slope of line connecting the mobility data points will be zero. Any slope of line falling between zero and one indicates the occurrence of SMR to some degree; a smaller value suggesting a more favorable SMR. Based on this deduction, we introduce a regression method to analyze the slope of line and use it as a means to qualitatively describe the SMR in the later discussion. These slopes are given in the Figures. In order to avoid congestion on the Figures making it difficult to distinguish the individual results, all of the straight line approximations have been omitted, except for the unity slope line through the "no surfactant" points. Distinctive symbols have been used, however.

Without the experimental error, the slope values of data sets in Fig.1-2 for CO_2-brine should be one as the total mobility of a two-phase mixture without surfactant is proportional to the rock permeability. In fact, the slope values of CO_2-brine were calculated to be 1.13 and 1.03, respectively for the two different core positions (as identified at the bottom of the plot). As the surfactant concentration increases, the slope of the mobility line decreases to 0.70, 0.77 (at 500 ppm) and 0.77, 0.81 (at 1000 ppm) for the two core positions. These slightly lower-than-one values for the slope indicate that the foam shows small amounts of SMR, which are at the just significant level. Although noticeable difference in slope values are found when core positions are changed, the difference is not significant in the interpretation of SMR. Therefore, but only for consistency, the remaining mobility measurements were conducted with the higher permeability core being placed ahead of the lower permeability core in the flow system.

When the mobility measurements were conducted with quarried rocks, SMR was observed in most cases when tests were completed with either surfactant CD1045 or CD1050. In the tests with the carbonate reservoir rocks, however, favorable SMR was not observed for both surfactants. This difference may have resulted from the remaining hydrocarbon residue in the cores, that interfered with foam formation, or may have been the result of larger-than-usual ongoing changes and erosion of the EVGSAU core during the test. In addition, it was found that the extent of SMR varied consistently among the other tests. Among several factors examined, the surfactant type and flow rate are found to be the two most significant parameters, while the rock type and surfactant concentration (so long as this was above the CMC) affect the SMR to a lesser extent.

A typical set of results showing the dependence of mobility on rock permeability is plotted in Fig. 1-3. Two groups of rocks included in this plot are Baker dolomite (ranging from 30 md to 110 md) and Berea sandstone (ranging from 130 md to 900 md). At a total flow velocity of 4.7 ft/day and regardless of rock type, the mobilities of CO_2-brine (depicted as solid squares) more or less fall on a line of unit slope when they are plotted against the sample permeabilities. In fact, the slope of this line as obtained from the regression shows a value of 0.95. As surfactant CD1050 concentration is increased from 0 to 500 ppm, the mobility of foam (shown as open diamonds) is significantly reduced. The slope of the line connecting these data points is reduced to 0.60, indicating that SMR occurs within the whole range of permeability. As the surfactant concentration is increased further, the mobility of foam is somewhat further reduced. However, the slope increases slightly — suggesting that additional surfactant does not improve SMR in this case.

Similar results are also plotted in Fig.s 1-4 to 1-6, in which mobility dependence is examined with a different type of surfactant and with different flow rate. In addition to these plots, the slope values as determined from the regression method are also tabulated in Table 1-1. Factors considered in this table include the flow rate, rock type, surfactant type and its concentration. By comparing the listed values, the slopes for most of CO_2-brine cases (0 ppm) are in the neighborhood of one. On the other hand, the slopes of most of foam cases are significantly less than one. As described previously, the slope value can be used as an indicator to show the extent of SMR among different cases. Therefore, surfactant CD1045 exhibits a slightly more favorable SMR in Berea sandstone than that in Baker dolomite (because the slopes in group of Berea sandstone cores are less than that in the

samples of Baker dolomite). Likewise, surfactant CD1050 exhibits a less favorable SMR in the Berea sandstone than in the Baker dolomite. In most cases, the increase of surfactant concentration improves the SMR when using surfactant CD1045, but fails to improve the SMR when surfactant CD1050 is used. Moreover, the results also reveal that a better SMR is exhibited at low flow velocity of CO_2-foam (4.7 ft/day) than at high flow velocity (9.4 ft/day) in all cases. This implies that SMR of foam may be improved when foam has traveled far away from the injection wells in the formation.

Unlike the results as found in the quarried rocks, however, a favorable SMR is not observed in the tests using dolomite reservoir rocks. The relationship between mobilities and rock permeabilities is displayed in Fig. 1-7. The mobilities of CO_2-brine fall approximately onto a unit slope line. The lines connecting mobilities of CO_2-foam for each surfactant, however, have slopes greater than one. Such a foam exhibits an unfavorable SMR by which its mobility is much higher in the higher permeability core than that in the lower permeability. This result contradicts what we have reported before,[2] and we will repeat the tests as necessary to resolve the uncertainty.

Based on the regression analyses of the data, we failed to observe an "ideal" SMR (a zero-slope line) of foam over the entire range of permeabilities. But if we narrowed the range of permeability under consideration, we could have identified some ideal SMR under certain conditions. For example, by using 500 ppm of surfactant CD1050 at a low flow velocity, the mobilities of foam are relatively similar with the rock permeability ranging from 50 md to 200 md (as shown in Fig. 1-3). On the other hand, by using 1000 ppm of surfactant CD1045 at a low flow velocity, the mobilities of foam are also almost constant with the rock permeability ranging from 70 md to 400 md (as shown in Fig. 1-5). Although under some circumstances foam exhibits an ideal SMR with a regression slope of zero, the Series 1 experiments have not been able to clarify just when this can be expected to occur.

Test Series 2

This work has been carried on in a somewhat different experimental circumstance. It has utilized fired Berea cores of 3.7 cm diameter and 7 cm length. These are somewhat larger than were used in the other laboratory. The permeabilities of the cores were 140, 490, and 985 md. Again, constant displacement pumps as sources of dense CO_2 and of surfactant-brine, and a smaller section of core was used as foam generator in which to mix the fluids. In this case, though, a commercial high-pressure back-pressure regulator (TEMCO BPR-50) was used to maintain the system pressure and to regulate the output fluids uniformly. The arrangement of experimental apparatus used in the Series 2 experiments is shown in Fig. 1-8. Two sets of steady-state experiments were conducted, investigating the effects of several parameters including rock permeability, flow rate, foam quality, surfactant type, and surfactant concentration. In the first of these sets of experiments, a constant CO_2:surfactant solution flow rate ratio of 4:1 was used. In the second set, the fixed ratio was broadened so that a wider range of foam quality (from 50% to 98.5%) was examined.

The results of this first set of experiments are described[4] completely in SPE 29168, where further details can be found. Two major conclusions are as given below. First, it is clear from these tests that varying degrees of SMR are consistently observed in Berea rock, with CD1045, CD1050 and Enordet X2001. SMR was not found, however, with another Chevron surfactant, CD1040. Because these experiments were purposely performed with larger size core samples, using a back-pressure regulator for control of pressure at the downstream end of the core, it was possible to make meaningful measurements prior to attainment of steady state, and to dispel any idea that the SMR observed in the Series 1 experiments might be an artifact of the small size of the core or the manner in which the experiments were conducted. By varying the flow ratio, we were also able to run tests over a much wider range of quality than has previously been performed.

Secondly, these tests provided an opportunity to explore and resolve an apparent difference between work at PRRC and foam experiments conducted at the University of California at Berkeley. In that work, not only was the quality of the foam higher — generally above 90% — but the flow of CO_2 or other gas and that of the aqueous liquid were regulated and varied separately. The pressure drops across the core sample thus were measured predominately as a function of the flow rate of one of the components, while the flow of the other fluid was held constant. Under these circumstances, as exemplified by a recent paper by Kovscek and Radke,[6] the measured pressure drops seemed mostly dependent on the liquid flow rate. At constant gas flow rates, the pressure increased about linearly as the flow of liquid was increased. On the other hand, at constant liquid flow rates, the pressure increased only slightly with increasing gas flow rate. In their tests, although the same pressure drop and flow data were taken, measurement of foam mobility was not the primary emphasis, and it was in fact not calculated.

In one series of our Series 2 tests, we employed similar procedures and separately varied the flow rates of CO_2 and of brine or surfactant solution. Results, in the high quality region, were generally quite similar to those obtained by Kovscek and Radke, with similar curves of pressure drop versus increasing CO_2 and surfactant rates. But when foam mobilities were calculated at the points

of overlap, the results were similar to those from our previous experiments.

CAPILLARY-CONTACT EXPERIMENTS

As described in the Introduction, our major task objective is to verify the existence of SMR with experiments in which both high and low permeability regions of cores are in capillary contact. For such experiments, core systems containing well-defined high and low permeability regions must be used; these must be arranged in the flow system as if these were different portions of a heterogeneous reservoir. We need to perform this type of experiment to verify the existence of SMR in more typical reservoir situations. With such a flow system, we will measure the ratio of mobilities of foams between the two sections as if they were flowing in different portions of a heterogeneous reservoir. We will also measure the ratio of mobilities between the two sections during the flow through these systems of simple fluids. Two types of such flow systems, parallel and series, are being considered and are under construction.

One type of experiment satisfying the above criterion involves cores in which high and low permeabilities are in parallel. Early in our work, we planned a test in which a core would be cut from a rock containing two regions, so that the plane separating the two includes the diameter of the core. End-to-end flows through the two sections can then be kept separate, so as to measure the two mobilities. Our search for samples, from which such parallel heterogeneity cores can be cut, has not yet produced any candidate cores from reservoirs. We nevertheless have two samples of quarried rock that meet this standard. One of these is a core we cut from a large San Andres carbonate outcrop sample (contributed by Texaco), but it unfortunately exhibits such a large permeability contrast across the geological demarcation plane that the experiment we contemplate would require an unduly long time to perform. A second choice would come from a block of Berea rock (on hand for another project) with greater-than-usual permeability heterogeneities. We expect to be able to cut a core from this block with a permeability ratio of 4 or 5, which will be more suitable for our tests.

Another parallel experiment is being performed in our Series 2 laboratory, with the two section coaxial. A 1.5 inch diameter Berea core has an axially located, 0.5 inch hole filled with fine unconsolidated sand. The steady-state pressure drop along the two sections is the same since they are in parallel, and again, the mobilities can be measured by observing the flow rates from the two regions separately. To properly perform this type of experiment, two back-pressure regulators are used; one is for the output fluids from each section of the core system. A schematic of the overall flow arrangement for this type of parallel experiment, which is at time being used for the coaxial flow described above, is shown in Fig. 1-9. Preliminary results and analysis of this experiment indicate that in steady state, some SMR *is* observed between the two parallel sections of the core — but that also an adjustment of the relative saturations occurs. Neither experiments or analysis on this parallel core system have been completed. This behavior, a change in the saturation conditions, has also been speculated by a study[7] in which the foam flowing behavior is related to the limiting capillary concept. These studies provide even greater motivation for experiments in which high and low permeability regions are in capillary contact, for more complete verification of laboratory-measured foam features,

so that they may be extended more credibly to field systems.

A second type of two-region experiment is a series arrangement, involving capillary contact between two measurable permeability regions. We have constructed such a composite core with two different permeability sections arranged in a series. In this new arrangement, the two sections of core are in the same coreholder. They could either be sections of the same rock or carefully-fitted separate cores, tightly butted together with a filter membrane for good capillary contact between them. A composite core of the latter type has been made in our lab by using two fired Berea sandstone cores, with air permeabilities of 100 md and 500 md. The coreholder to contain such a core has also been fabricated. This coreholder is equipped with five pressure taps capable of measuring four pressure drops along the flow path. In this case, two pressure drops across each section of the composite core can be measured at the same time. After a steady state has been reached during the mobility measurement, it will be possible to compare the mobilities of fluid flowing through the two sections.

Pressure measurements for this experiment will be especially critical. We are extremely grateful to Amoco Production Company for a recent donation of a number of Honeywell pressure transmitters (or transducers) which we shall use in this experiment. We are currently testing and assembling these new pressure transmitters, and the electronic current sources and measuring resistors we have assembled for them. The use of these new transducers in our experimental setup will improve the precision of our measurements. We will start to conduct such experiments once the system is completely constructed.

CONCLUSIONS

During the first year of the project, our activities on this task have produced several results of interest.

1. After examining the experimental setup for measurement of mobility of two cores in separate coreholders, we have found that the position of the cores does not show significant effect on the interpretation of SMR in mobility measurements.

2. Measuring CO_2-foam mobility in separate cores, selective mobility reduction is affected significantly by the surfactant type and the flow velocity of foam. Rock type and surfactant concentration also affect the SMR of foam, but only to a lesser extent.

3. SMR is found to be more favorable in Baker dolomite rocks than in Berea sandstone, when surfactant CD1050 is used as a foamer. When surfactant CD1045 is used as a foamer, however, SMR is found to be more favorable in Berea sandstone than in Baker dolomite rocks.

4. In most cases, better SMR is exhibited at a lower flow velocity of foam.

5. Extensive mobility measurements on larger Berea cores have been made, with results similar

to those obtained with smaller cores.

6. Two types of parallel region mobility comparison and one series arrangement, are in various states of preparation. These are needed to test whether capillary contact between high and low permeability regions will have any effect on the occurrence or magnitude of Selective Mobility Reduction.

REFERENCES

1. Lee, H.O., Heller, J.P., and Hoefer, A.M.W.: "Change in Apparent Viscosity of CO_2-Foam with Rock Permeability," paper SPE 20194 presented at the SPE/DOE 8th Symposium on Enhanced Oil Recovery, Tulsa, April 22-25, 1990, *SPERE* (Nov. 1991) 421-428.
2. Tsau, J.S. and Heller, J.P.: "Evaluation of Surfactant for CO_2-Foam Mobility Control," paper SPE 24013 presented at the 1992 Permian Basin Oil and Gas Recovery Conference, Midland, March 18-20.
3. Dixit, A., Tsau, J.S., and Heller, J.P.: "Laboratory Study on Surfactant-Based Selective Mobility Control," paper SPE 27729 presented at the 1994 Permian Basin Oil and Gas Recovery Conference, Midland, March 16-18.
4. Yaghoobi, H. and Heller, J.P.: "Laboratory Investigation of Parameters Affecting CO_2-Foam Mobility in Sandstone at Reservoir Conditions," paper SPE 29168 presented at the 1994 SPE Eastern Regional Meeting, Charleston, Nov. 8-10.
5. Yang, S.H. and Reed, R.L.: "Mobility Control Using CO_2 Foams," paper SPE 19689 presented at the 1989 SPE Annual Technical Conference, San Antonio, Oct. 8-11.
6. Kovscek, A.R., and Radke, C.J.:"A Comprehensive Description of Transient Foam Flow in Porous Media," prepared for the DOE/NIPER Symposium on Field Application of Foams for Oil Production, Bakersfield, CA, Feb. 11-12, 1993.
7. Khatib, Z.I., Hirasaki, G.J., and Falls, A.H.: "Effects of Capillary Pressure on Coalescence and Phase Mobilities in Foams Flowing Through Porous Media," *SPERE* (Aug. 1988) 919-926.

Table 1-1. Slopes determined by the regression from the mobility measurements.

Flow rate (cc/hr)	Rock type	Surfactant CD1045			Surfactant CD1050		
		0 ppm	500 ppm	1000 ppm	0 ppm	500 ppm	1000 ppm
7.5	Berea sandstone	1.09	0.30	0.36	1.03	0.71	0.76
	Baker dolomite	0.94	0.61	0.45	0.97	0.23	0.45
	Overall	0.82	0.39	0.26	0.95	0.60	0.65
15	Berea sandstone	1.12	0.45	0.34	1.16	0.72	0.72
	Baker dolomite	1.12	0.83	0.56	0.92	0.55	0.45
	Overall	0.90	0.49	0.34	0.99	0.67	0.70

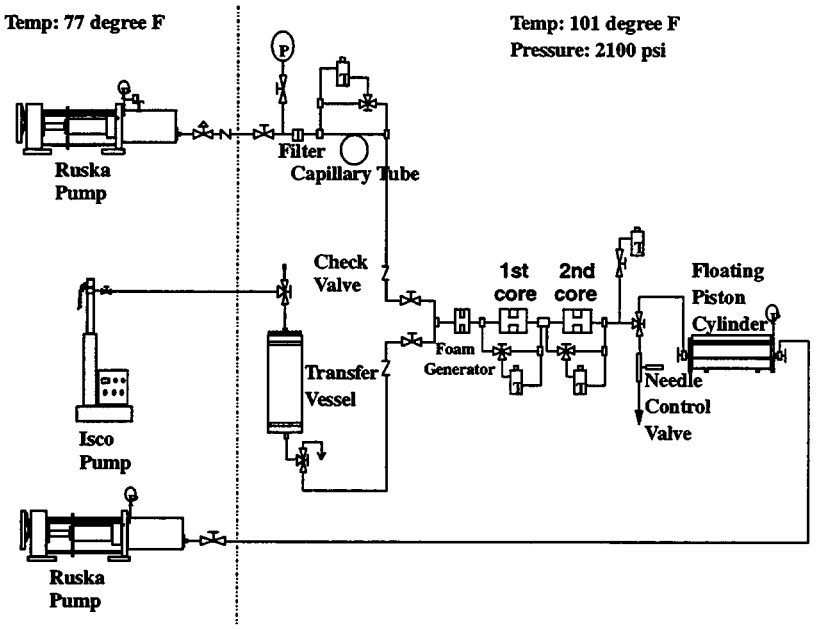

Fig. 1-1. Schematic of the mobility measurement experimental setup.

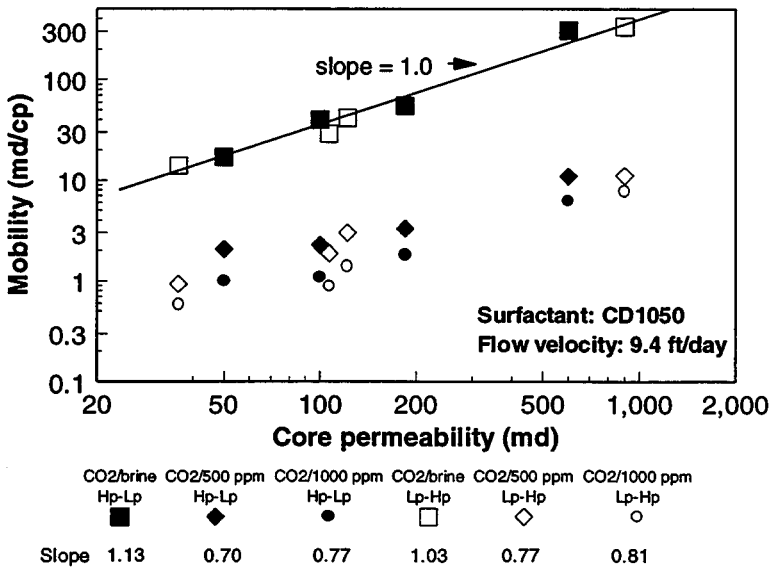

Fig. 1-2. Effect of core position on the mobility measurements.

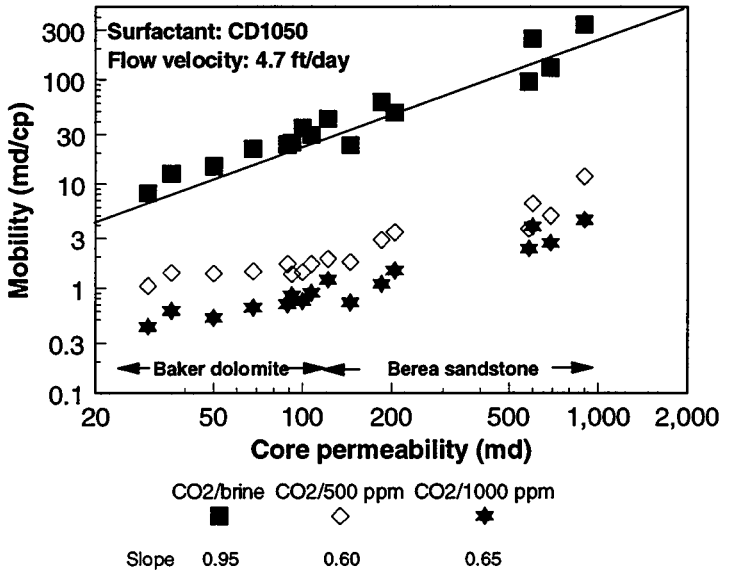

Fig.1-3. Dependence of mobility on permeability.

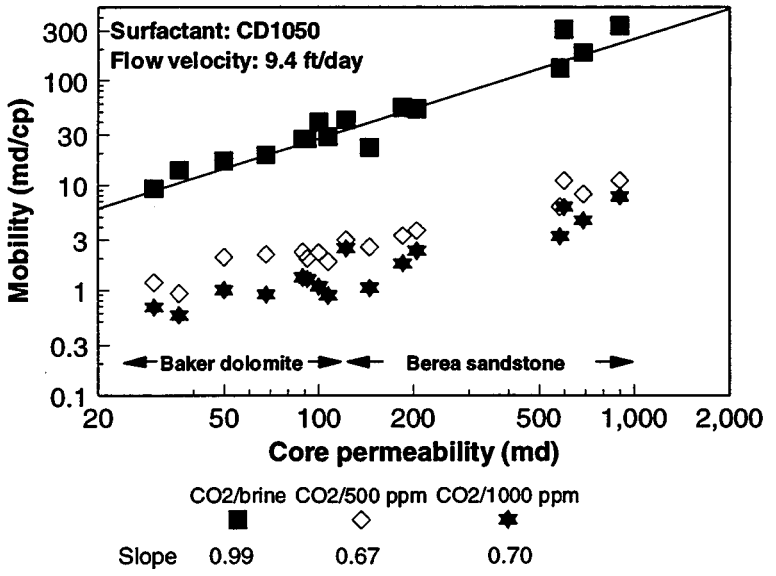

Fig. 1-4. Dependence of mobility on permeability.

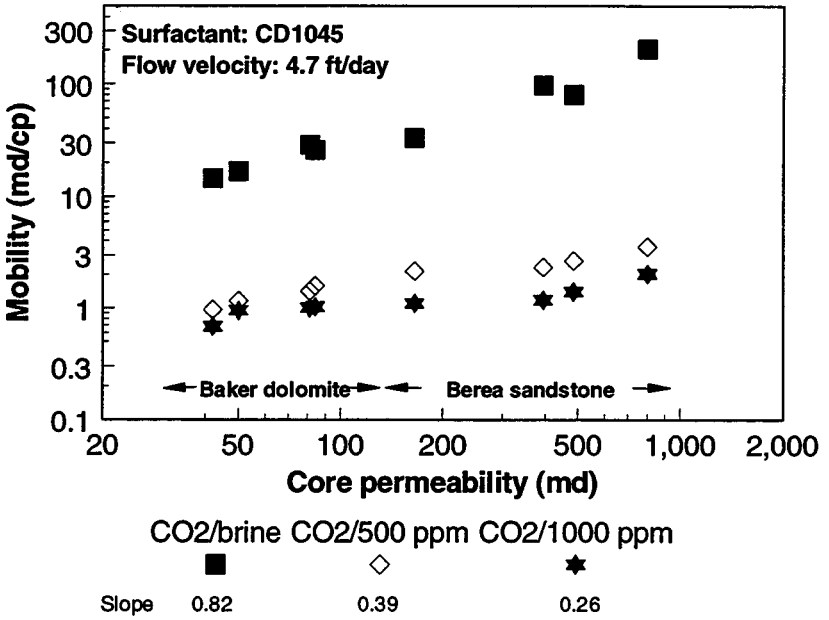

Fig. 1-5. Dependence of mobility on permeability.

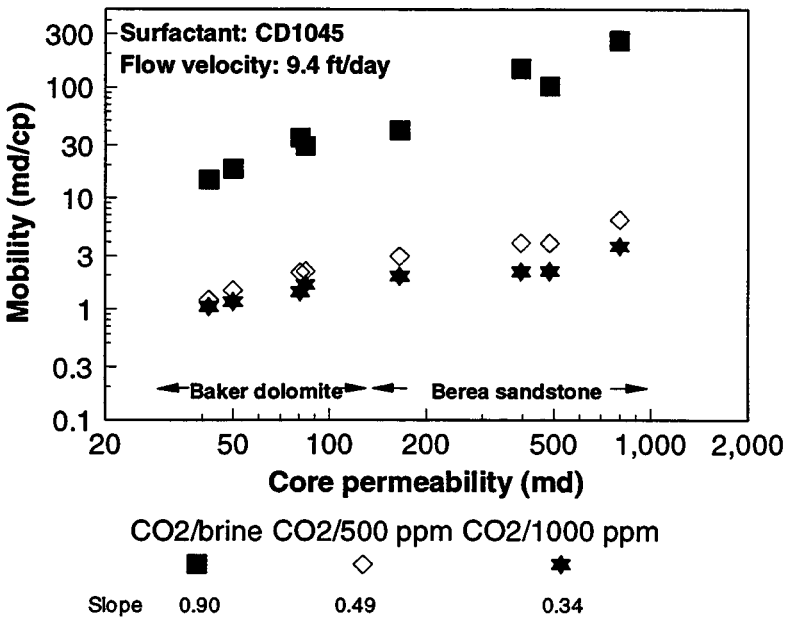

Fig. 1-6. Dependence of mobility on permeability.

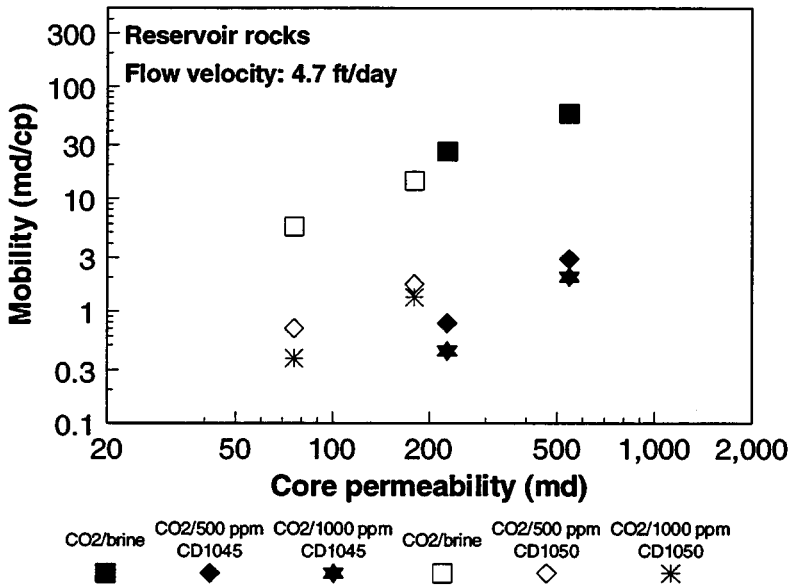

Fig. 1-7. Dependence of mobility on permeability.

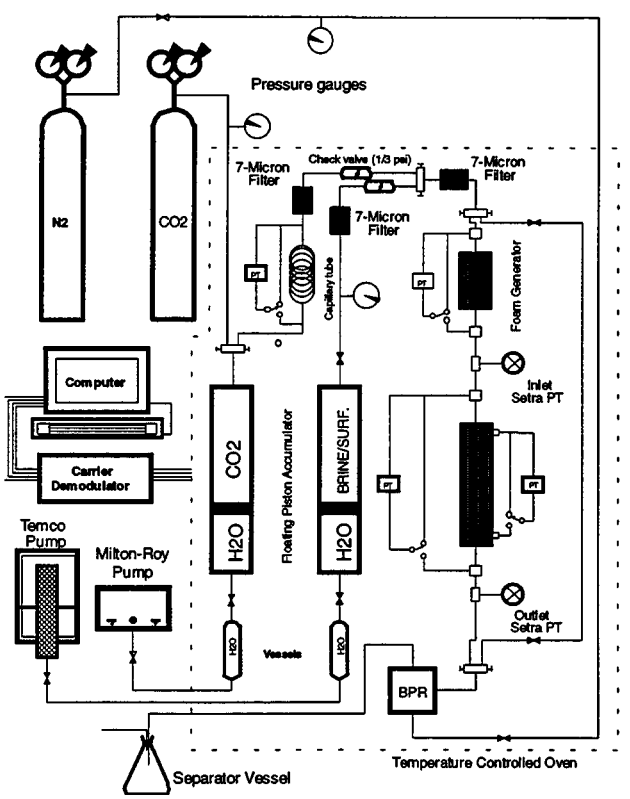

Fig. 1-8. Schematic diagram of the experimental apparatus (phase one).

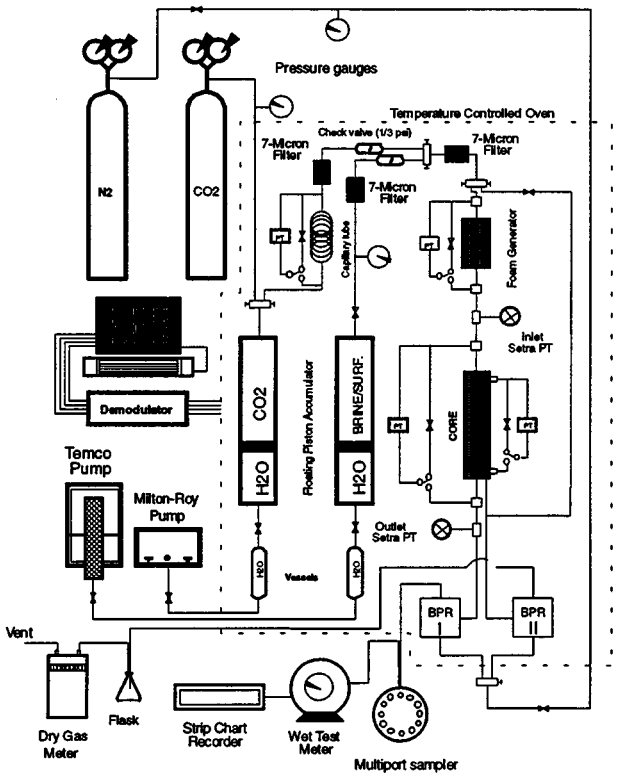

Fig. 1-9. Schematic diagram of the experimental apparatus (phase two).

TASK 2: REDUCTION OF THE AMOUNT OF CO_2 REQUIRED IN CO_2 FLOODING

INTRODUCTION

A multitude of successful gas injection projects throughout the world[1] have demonstrated that high pressure CO_2 injected into oil reservoirs does improve oil recovery. It is not a question of whether CO_2 improves oil recovery, but of improving the economics of injection projects. These projects require significant expenditures for the purchase of CO_2 and the facilities for handling and transporting CO_2 years before increased oil recovery is realized.

In a review article by Hadlow[2] on the industry's experience with CO_2 injection, he says, "One of the most significant opportunities for expanding the use of CO_2 could be the application of CO_2 flooding in reservoirs in which near miscible conditions exist." Two field examples are given where CO_2 was used to pressure the reservoir and a good reservoir response to CO_2 injection was seen below the minimum miscibility pressure (MMP). Thus, by decreasing the amount of CO_2 required per unit of oil produced and/or by increasing the sweep efficiency of the CO_2, the unit cost of producing oil decreases.

BACKGROUND

At a constant temperature the density of CO_2 decreases with decreasing pressure, thus increasing reservoir fill volume with the same mass. At some pressures, the change in density over a relatively small pressure range is substantial, see Fig. 2-1. This effect is common near the MMP of many reservoirs. A concern of many is what happens to the sweep efficiency of a CO_2 flood as the system pressure is reduced to the MMP, and more importantly, below the MMP. Recovery in slim tube tests, a common method of determining the MMP for a oil-injection gas system, is essentially flat above the MMP, but decreases significantly as the pressure is reduced below the MMP. The porous media of a slim tube is made up of a sand or glass bead pack and contains no water saturation, which is quite different from the reservoir. This brings up a pertinent question: does the drastic reduction in oil recovery as the pressure decreases below the MMP in a slim tube test occur in a reservoir, and if it does, can the reduced oil recovery be economically minimized?

As the effect of pressure on recovery is studied, both support for and against the rapid reduction in recovery below the MMP have been found. After all the laboratory work is done, the concepts must be tested in the field. This requires field data and models to simulate what is occurring in a reservoir. As part of this work, we are improving current concepts on fluid flow and incorporating them into reservoir models. Mechanisms such as foam generation, pressure, well orientation, and injection scheme must be tested using the reservoir model.

EXPERIMENTAL TESTS

A number of tests can be performed, in which each has a function in understanding displacement mechanisms, but are not exactly under exact reservoir conditions. Several of these tests

have been done over the last year. One oil that we are running a number of tests on is from a Spraberry Reservoir. This reservoir is of interest as a candidate for CO_2 flooding and as a fractured reservoir where members of the PRRC have a related project. This oil was also selected as the oil, with a reservoir temperature (above 120°F), that is too high to have three hydrocarbon-CO_2 phases at high CO_2 concentrations. Other oils that were tested this past year because of previous tests done in this laboratory were Maljamar[3] and Wasson.[4] Again, the main focus in this task is recovery mechanisms that are affected by pressure.

Slim Tube Tests

Slim tube tests were done in a 40 ft. long 0.25 inch ID with a pore volume of 117.9 cm^3, see Fig. 2-2 for the schematic of the slim tube system. The indicated test pressure is the pressure at the inlet of each slim tube test. The inlet pressure was controlled by changing the pressure of the back pressure regulator at the outlet side of the slim tube. The injection rate of the CO_2 high-pressure gas was 30 cm^3/hr.

Fig. 2-3 shows a series of slim tube test results with percent recovery indicated after 1.187 and 1.527 pore volumes (PV) of CO_2 injected into the slim tube in each case. The tests are differentiated by the pressure of each test. These tests were run on Spraberry separator oil at 138°F (reservoir temperature). Note that above 1550 psig, there is little increase in recovery especially when comparing tests at 1.187 PV of CO_2 injection, while below 1550 psig there is a significant pressure effect on recovery. About 1550 psig is considered to be the MMP. Data from each individual run can be obtained from the PRRC upon request.[5] The measured MMP is lower than the bubble point pressure might be in some parts of the reservoir. The bubble point pressure is believed to be as high as 1900 psig in parts of the reservoir. Thus the MMP should be considered to be the higher of 1550 psig or the bubble point pressure. Each test was conducted for 420 minutes with volume of oil produced and grams of CO_2 injected recorded every 20 minutes, and pressure drop across the core every 6 minutes.

Slim tube tests on Maljamar oil were performed at 1400 and 1600 psig at 140°F. At both pressures, the recovery was lower than for Spraberry at similar pressures. The temperature was only two degrees higher. The API gravities of the two oils are quite similar. The big difference was that the Maljamar oil was not a separator oil that had been maintained under pressure, thus it was a weathered sample from which some of the intermediate components had evaporated. In developing multi-contact miscibility, the intermediate components (especially hexanes through decanes) that are lost due to evaporation upon weathering are critical.

In other slim tube tests[6] and micromodel studies[7] when plotting recovery versus grams of CO_2 injected or the recovery efficiency (mass of oil produced per mass of CO_2 injected), the combination of high recovery and mass of CO_2 required to produce a given volume of oil is best near the MMP. Fig. 2-4 compares results of Maljamar separator oil displaced by dense CO_2 gas at 90°F for several micromodel tests[7] versus pressure: the most efficient displacement was at 1000 psia, which is essentially the MMP in the system. At higher pressures, the final recovery was about the same, but

the mass of CO_2 required to file the pore volume was greater because of the higher density.

Core Tests

Micromodels and slim tubes are not reservoir rock and are usually not at near-reservoir dimensions. The micromodel is a small two-dimensional system that can have oil, gas, and water present, with that system in glass. It is very interesting to see the two-dimensional flow and some of the mechanisms that are sure to be present in reservoir systems, but only so much can be learned. Then in the slim tube tests, they are essentially one-dimensional and contain no water. These limitations can be reduced by core floods, using reservoir rock, developing the proper reservoir models in order to simulate the reservoir floods, and matching the reservoir model to actual reservoir data.

Even though slim tube data indicate a sharp production drop below the MMP, some reservoir data[2] and laboratory core floods[8] have indicated that the drop off is not nearly as sharp in reservoir rock. This could well be due to reservoir heterogeneities, reservoir dimensions, water present in the system, and/or multi-phase flow (up to four possible phases). But there are also core flood tests that have been done at the PRRC and elsewhere that indicate that the recovery reduction below the MMP might be significant and similar to the slim tube production reduction as pressure decreases. Figure 2-5 is an example of the results of the amount of the oil produced from the core. Both production at 1.2 and 2.0 PV of CO_2 are indicated. The oil was a synthetic oil of decane and hexadecane. All these tests were done at 93°F. Around the MMP in the 1200 to 1300 psig range, there is a definite reduction in recovery. This is unlike some work reported in the literature[8] that indicated a less obvious reduction due to pressure drop. The difference can be contributed to oil composition, flooding conditions, and upstream processes on the injection fluid.

CO_2 Swelling Tests

CO_2 gas was injected into a PVT cell that contained live Spraberry oil. The live oil was prepared by combining separator gas and oil to approximate a reservoir oil with a bubble point pressure of 1900 psig. Figure 2-6 compares the composition of the separator oil used in the slim tube tests with the live oil used in the swelling tests. Figure 2-7 is a summary of the constant composition volume expansion tests. Seven tests were done with the added CO_2 content ranging from zero to 73 mole percent. The constant volume contour lines were calculated using the measured phase volumes versus pressure data taken at each CO_2 concentration. The experimental phase volumes, compositions, and densities can be obtained from the PRRC in PRRC Report 95-21.[5]

Continuous Phase Equilibrium Tests

The PRRC's continuous phase equilibrium (CPE) apparatus was used to obtain composition, density, and viscosity for a West Texas recombined crude oil (Wasson) during the injection of high pressure CO_2, which was continuously injected at constant pressure and flow rate. The system is maintained at constant pressure during CO_2 injection by controlling the production rate.

Compositions, densities, and viscosities of the produced fluids were determined at system pressure and temperature, providing continuous monitoring of fluid properties produced at outlets at both the top and bottom of the CPE apparatus.

The tests were run using both pure and impure CO_2 at 105°F and pressure ranging from 1200 to 2500 psig. The MMP of the system is about 1350 psig for pure CO_2. Impurities added to the injection gas were methane, ethane, and propane. The solubility of the injected CO_2 in the oil-rich phase was found to have little dependence on pressure, while the solubility of hydrocarbons in the CO_2-rich phase increased with increasing pressure. Impurities in the injected CO_2 did not significantly affect trends in composition, density, and viscosity of each phase. More detail can be found in paper SPE 28974, "Dynamic Phase Composition, Density, and Viscosity Measurements During CO_2 Displacement of Reservoir Oil.[9]" Also, all experimental data is available upon request from the PRRC.[10]

Discussion of Experimental Tests

The tests described here can be used for a number of purposes. These include understanding flooding mechanisms and pressure effects. The results can also be used to tune equations of state that are then in turn used to predict results as the systems change due to dynamic compositional changes occurring in real systems. These are then used to model and understand behavior on a reservoir scale.

SIMULATION

With the always-present concern that recovery-mechanism efficiencies are greatly reduced below the MMP, even though the extent is under consideration, it is wise to look for mechanisms that would counter the reduction. These can include both foams and other methods such as horizontal wells. Thus, when developing models to simulate reservoir flow development, the models should include foam features and various injection methods such as horizontal wells. CO_2-foam has been studied in previous laboratory work[11-14] and field foam tests [15-17] done by the PRRC. Also, the reservoir models to simulate mass transfer in CO_2 floods require compositional transfer capabilities that require considerable phase behavior development.

Phase-Behavior Prediction Simulations

Compositional models based on cubic equations of state[18] are generally employed for simulation of the reservoir performance in CO_2 flooding processes. Generally, with a large number of pseudo-components used in characterizing the heptanes-plus (C_{7+}) fraction of an oil, a satisfactory prediction of the phase behavior can be obtained. In compositional models, however, the cost and computing time can increase significantly with the increased number of components in the system. Therefore, there are limitations on the maximum number of components that can be used in compositional models and the original multicomponents in an oil have to be lumped into a smaller

number of pseudo-components. That is one of the objectives of C_{7+} characterization: to obtain the best possible description of the C_{7+} fraction using a minimum number of pseudo-components. Tuning of the equation-of-state parameters to experimental equilibrium data generated at static conditions prior to the reservoir simulation studies is the current practice in the industry. One objective of this work was to set up a preprocessor program to generate input parameters for compositional simulators. In this preprocessor program, the equation-of-state parameters and other parameters such as the average molecular weight of the C_{7+} fraction are tuned to match the equilibrium data generated at static conditions. A compositional model which is tuned to these static data, nevertheless, may not be adequate to predict the phase behavior around the critical region or close to the minimum miscibility pressure. This is still an important issue which merits special attention.

Currently, the preprocessor is able to match the bubble-point pressure data by tuning the average molecular weight of C_{7+} fraction. After matching the bubble-point pressure, the preprocessor program will generate parameters that can be used as input to compositional simulators. Our goal is to improve the preprocessor to match not only the bubble-point pressure data but also other equilibrium data generated at static conditions.

During the development of the preprocessor program, a new and effective method was proposed for estimating the specific gravities of pseudo-components that are required to characterize the heavy components of crude oils. This method uses the most often available data of the heavy components of crude oils: average molecular weight and specific gravity of the C_{7+} fraction. The proposed method makes use of the definition of the Watson characterization factor, which is the cube root of boiling point in Rankine (°R) divided by specific gravity, and the corrected Riazi-Daubert relation for the boiling point[19]:

$$T_{bi} = \frac{6.77857\ M_i^{\ 0.401673}\ \gamma_i^{\ -1.58262}}{\exp[\ -\ (b\ M_i\ +\ c\ \gamma_i\ +\ d\ M_i\ \gamma_i)]}$$

where T_{bi} is the boiling point (°R), γ_i is the specific gravity (at 60 °F relative to water at 60 °F), and M_i is the molecular weight of the pseudo-component, and constants b, c, and d are equal to 0.00377409, 2.984036, and -0.00425288, respectively. Using the definition of the Watson characterization factor, K_W, the specific gravity of the pseudo-component is given as:

$$\gamma_i = \frac{T_{bi}^{\ 1/3}}{K_w}$$

By solving the above two equations with the successive substitution method, we can obtain the

specific gravity of the pseudo-component. If the calculated average specific gravity of the C_{7+} fraction does not match the measured value, a new value of the Watson characterization factor is calculated using the Newton method. The whole calculation is iterated until a value of the Watson characterization factor gives specific gravities of pseudo-components that can match the measured value. In order to evaluate the new method and compare it with the existing estimation methods, a procedure has been implemented, without using any tuning techniques, for the phase equilibrium predictions of crude oil-CO_2 systems. The phase equilibrium predictions, based on the specific gravities estimated by the new method and the existing methods proposed by Whitson et al.[20] and Yarborough,[21] were all reasonably accurate and of the same magnitude. The specific gravities estimated by the new method and the method proposed by Whitson et al.[20] always provided similar phase behavior predictions. A paper,[22] entitled "Characterization and Multiphase Equilibrium Prediction of Crude Oil Heavy Components," which described in detail the proposed method and comparisons with the existing methods, was presented at the 1995 AIChE Spring National Meeting held in Houston, March 19–23.

CO_2-Foam Simulations

Work has been conducted on incorporating CO_2-foam features into reservoir simulators. The reservoir simulators used in this work include a multi-component pseudo-miscible reservoir simulator, MASTER (Miscible Applied Simulation Techniques for Energy Recovery), obtained from the Department of Energy and a compositional reservoir simulator, UTCOMP, graciously provided by Dr. Gary Pope of the University of Texas at Austin.

A foam model has been developed by utilizing the tracer features in UTCOMP. The surfactant solution movement is tracked by treating the surfactant solution as an aqueous tracer without the addition of a surfactant-solution conservation equation into UTCOMP. [The tracer adsorption model has been modified to account for the adsorption isotherm.] Instead of using a mechanistic, bubble-population-balance approach[13, 23-25] to calculate the mobility of the gas-foam phase, the foam model reads, as input, the foam-resistance-factor data as lookup tables. The resistance factor is treated as a function of interstitial velocity, gas-liquid volumetric ratio, and surfactant concentration based on laboratory test results. In order for foam to exist, the following conditions must be satisfied:

$$S_g > S_g^{\lim},\ S_o < S_o^{\lim}$$

$$C_s > C_s^{\lim},\ S_w > S_w^{\lim}$$

where S_g, S_o, and S_w are the gas-, oil-, and water-phase saturations, respectively, and C_s is the surfactant concentration. The variable with superscript *lim* corresponds to the limiting value of each variable. If any one of these conditions is not met, foam is not formed and the gas-phase mobility is not modified. By assuming foam has no effect on the water phase, the mobility of the gas-foam phase

is calculated according to

$$M_g^{\text{foam}} = \frac{1}{R_f}\left(M_w + M_g\right) - M_w$$

where M_w is the water-phase mobility, M_g is the foam-free gas-phase mobility, and R_f is the resistance factor which is defined as

$$R_f = \frac{M_{CO2+BR}}{M_{CO2+SS}}$$

Here, M_{CO2+BR} is the mobility obtained from the experiment of simultaneous injection of CO_2 and brine, M_{CO2+SS} is the mobility obtained from the experiment of simultaneous injection of CO_2 and surfactant solution, and both measurements are conducted at the same gas-liquid volumetric ratio. The resistance factor can represent the pressure drop attributed to the presence of foam.Without foam, the resistance factor would be unity. The mobility of the gas-foam phase is calculated after the foam resistance factor is determined from lookup tables.

The major modifications that were made to MASTER include (1) the addition of two conservation equations to permit simulation of surfactant solution and foam bubble, (2) the addition of an algorithm to calculate the mobility of gas-foam phase, and (3) the addition of a foam-resistance-factor table-lookup option similar to the one that has been incorporated into UTCOMP. In this new foam-flood simulator, the mobility of gas-foam phase can be calculated by two approaches. The first approach uses the foam-bubble population balance equation and the second approach uses the foam-resistance-factor table-lookup option. The foam features can be easily bypassed in the simulator, giving essentially the original MASTER model, which can be used to simulate a wide range of immiscible-to-miscible gas-injection recovery processes. In addition, the simulator can be used to simulate most of the common primary and secondary recovery mechanisms by bypassing both the foam and miscible features in the model.

Simulation tests on a three-dimensional quarter of a five-spot pattern have been performed to assess the sensitivity and adequacy of the included foam features in UTCOMP. The reservoir is divided into five layers and the reservoir model description is as follow:

Grid:

- Reservoir size: 660 ft x 660 ft x 160 ft (20-acre well spacing)
- Grid geometry: 8 x 8 x 5
- Grid block size in the x and y directions (constant size): 82.5 ft
- Grid block size in the z direction: 27, 40, 35, 18, 40 ft
- Well radii: 0.33 ft

Rock Properties:

- Porosity of each layer: 0.1, 0.06, 0.08, 0.15, 0.07
- X-direction permeability of each layer: 150, 70, 112, 1000, 70 md

Y-direction permeability of each layer: 150, 70, 112, 1000, 70 md
Z-direction permeability of each layer: 15, 7, 11.2, 100, 7 md

Operation Condition:

Injection well is perforated at the whole layers and maintained at constant molar injection rate: 2500 lb-moles/day water during water injection
800 lb-moles/day CO_2 during CO_2 injection

Production well is perforated at the whole layers and limited at bottom-hole pressure of 1500 psia at the first layer

The initial conditions for foam tests were established by simulating a 10-year water flood and a 5-year CO_2 flood from an initial pressure of 1500 psia and an initial water saturation of 25%. The foam test is performed using the following injection schedule:

(1) Surfactant (2500 ppm active) injection for 122 days.
(2) Rapid SAG injection of 6 SAG cycles for 90 days. A SAG cycle consists of 3-days of surfactant solution and 12-days of CO_2.
(3) CO_2 injection for 153 days.

This injection schedule is specifically selected to mimic the injection schedule used in EVGSAU CO_2-foam pilot test.[26]

In order to evaluate the foam test, a base case simulation was performed. In this base case, the injection schedule is identical with that of the foam test except surfactant solution is replaced with surfactant-free brine. Figure 2-8 shows the oil rate history for the foam test and the base case. Observe the significant increase in the oil rate from about 10 STB/D to about 85 STB/D, commencing from about 320 days for the foam test compared to the base case. To understand the results better, the injection profile for the two cases at 236 days of simulation are shown in Fig. 2-9. Layer 4 is the most permeable layer with a permeability of 1000 md, while layers 2 and 5 are the least permeable at 70 md. Figure 2-9 shows that, at the base case, most of the injected CO_2 would be injected through the highest permeability layer, while the least amount of CO_2 would be injected through the least permeable layers. Consequently, the sweep efficiency is poor and the oil rate is low. However, for the foam test, there were significant increases in the amount of CO_2 injected through layers 2 and 5. At the same time, the amount of CO_2 injected through layer 4 was reduced by half. Therefore, due to the presence of the foam, the profile modification significantly improved the sweep efficiency, resulting in a higher oil rate.

The effect of the magnitude of the foam-resistance factor on the oil rate was examined by using a scaling parameter F. As shown in Fig. 2-10, the response to the foam for the oil rate to increase was delayed when the magnitude of the foam-resistance-factor data was scaled down by the parameter F. Sensitivity study of one of the parameters that determine the existence of foam, S_g^{lim}, has also been performed. When gas saturation is less than S_g^{lim}, foam cannot exist. Figure 2-11 shows the simulation results when S_g^{lim} (SGLIM) equals to 0.15, 0.2, 0.25, and 0.3, respectively. When S_g^{lim} increases, the response to the foam was delayed. The oil production rate for the case when S_g^{lim} equals to 0.15 increased to a peak and then dropped and leveled off at a higher oil rate.

This kind of response is similar to that was observed in the offending well of the EVGSAU field pilot test as shown in Fig. 2-12.[17] When S_g^{lim} increases from 0.15 to 0.2, the response to the foam was similar but delayed. When S_g^{lim} increases from 0.25 to 0.3, the response to the foam was not observed during the period of investigation and the results plotted in Fig. 2-11 were identical to that of the base case for this period.

In summary, the results to date have shown that the effects of foam that were observed in the field can be simulated using the foam-resistance-factor table lookup approach. The response to foam can be controlled by adjusting the limiting gas saturation and the scaling parameter F, both of which are presently under investigation.

Horizontal-Well Simulations

To successfully apply horizontal wells to CO_2 flooding, reliable and accurate tools are needed to aid in the design and performance predictions of such projects. A reservoir simulator with horizontal well capabilities can provide guidance into the design of well lengths, locations, and other process parameters associated with horizontal wells. Simulation is also a relatively inexpensive and reliable way to predict the performance of horizontal wells under actual field conditions.

A multi-component pseudo-miscible reservoir simulator, MASTER, obtained from the Department of Energy, has been debugged and used to study CO_2 flooding processes at the PRRC. In addition, MASTER has been modified to include the bubble population balance approach[13] and the resistance factor table-lookup approach (discussed in previous section) for foam modeling. However, MASTER was only able to handle vertical well simulations, that is, only the vertical well parallel to the z-axis was considered in MASTER. One objective of this research was to incorporate horizontal well modeling capability into MASTER.

We have implemented Babu *et al.*,[27] the equivalent wellblock radius formulation, into the MASTER, because the equation is general and is valid for both vertical and horizontal wells, for any well location, and for any anisotropy. Furthermore, the equation is still accurate for anisotropic grids of high aspect ratio whereas Peaceman's equations require modifications. In the original MASTER code, the well was represented only as a vertical well parallel to the z-axis. The wellblock productivity index were input from the users. Therefore, the first task was to modify the code to allow for flexible well orientation, i.e., wells can be parallel to the x-axis, y-axis, or z-axis. Horizontal wells are parallel to the x- or y-axes, whereas vertical wells are parallel to the z-axis. The wells can not be inclined. The second major modification involved incorporating Babu *et al.*'s[27] well model into the simulator. For a detailed description of the general analytical formula for the equivalent wellblock radius, we refer the reader to the original papers.[27]

In summary, major modifications that were made to MASTER include (1) allowing flexible well orientations, i.e., wells can be parallel to the x-axis, y-axis, or z-axis, and (2) incorporating Babu *et al.*'s[27] well model into the simulator. The coding of these modifications has just been completed.

CONCLUSIONS

1. The CO_2 MMP with Spraberry separator oil is 1550 psig. This will also be appropriate for Spraberry reservoir oil unless the bubble point pressure is above 1550 psig. To prevent the formation of a large immiscible methane bank, gas injection should be done above the bubble point pressure.

2. It is critical to prevent weathering before tests such as MMP determinations.

3. Recovery versus pressure has been examined in tests from the literature and work done at the PRRC. These results in some cases have recovery reductions very similar to slim tube tests, but in others the recovery is much less pronounced. The cause of these differences are not fully understood.

4. A detailed Px phase diagram has been completed for the CO_2-Spraberry recombined reservoir (live) crude system. This system has a saturation curve that includes bubble point pressure, dew point pressures, and estimated critical point. Also shown are the constant volume contour lines estimated from measured phase volume data.

5. Continuous phase equilibrium tests on Wasson crude with both pure and impure CO_2 and below and above the MMP using recombined reservoir crude found pressure effected the solubility of oil in CO_2 much more than CO_2 in oil.

6. A preprocessor for reservoir compositional simulators has been developed to match the bubble-point pressure data by tuning the average molecular weight of the C_{7+} fraction.

7. A CO_2-foam option using look-up tables has been added to two reservoir simulators used for CO_2-miscible flooding. These are a debugged version of DOE's MASTER and the University of Texas Austin's UTCOMP.

8. A CO_2-foam option using a foam-bubble population balance equation has been incorporated in MASTER.

9. MASTER has been modified to include horizontal well capabilities.

Future Work

Future work in this task area will include: 1) MMP determination, continuous phase equilibrium test, and CO_2-swelling test on at least one system during the next year, 2) process and pressure effects on core flood tests, 3) core foam tests versus pressure, 4) continued development of phase behavior preprocessor for reservoir simulation, including other static cell phase equilibrium data besides bubble point pressure, 5) testing the CO_2-foam option in both MASTER and UTCOMP, using the East Vacuum CO_2-foam pilot test as a confirmation run, and 6) testing the horizontal well option in MASTER.

REFERENCES

1. Martin, F.D.: "Enhanced Oil Recovery For the Independent Producer," paper SPE/DOE 24142 presented at the 8th Symposium on Enhanced Oil Recovery, Tulsa, April 22-24, 1992.
2. Hadlow, R.E.: "Update of Industry Experience with CO_2 Flooding," paper SPE 24928 presented at the 67th SPE Annual Technical Conference and Exhibition, Washington, D.C., Oct. 4-7, 1992.
3. Orr, F.M., Jr., Silva, M.K., and Lien, C.-L.: "Equilibrium Phase Compositions of CO_2/Crude Oil Mixture-Part 2: Comparison of Continuous Multiple-Contact and Slim-Tube Displacement Tests," *SPEJ* (April 1983) 281-291.
4. Lansangan, R.M. and Smith, J.L.: "Viscosity, Density, and Composition Measurements of CO_2/West Texas Oil Systems," *SPERE* (Aug. 1993) 175-182.
5. Grigg, R.B., Kernodle, J.L., and Onimole, A.: "Data from Minimum Misciblity and CO_2 Swelling Tests for Spraberry Crude," PRRC Report 95-21, New Mexico Petroleum Recovery Research Center, May 1995, Socorro, NM.
6. Creek, J.L. and Sheffield, J.M.: "Phase Behavior, Fluid Properties, and Displacement Characteristics of Permian Basin Reservoir Fluid/CO_2 Systems," *SPERE* (Feb. 1993) 34-42.
7. Chang, S.-H., Martin, F.D., and Grigg, R.B.: "Effect of Pressure on CO_2 Foam Displacements: A Micromodel Visualization Study," paper 27784 presented at the SPE/DOE Ninth Symposium on Improved Oil Recovery, Tulsa, April 17-20, 1994.
8. Shyeh-Yung, J.J.: "Mechanisms of Miscible Oil Recovery: Effects of Pressure on Miscible and Near-Miscible Displacement of Oil by Carbon Dioxide," paper SPE 22651 presented at the 1991 SPE Annual Technical Conference and Exhibition, Dallas, Oct. 6-9.
9. Grigg, R.B.: "Dynamic Phase Composition, Density, and Viscosity Measurements During CO_2 Displacement of Reservoir Oil," paper SPE 28974 presented at the 1995 SPE International Symposium on Oilfield Chemistry, San Antonio, Feb. 14-17.
10. Grigg, R.B. and Fritchman, D.M.: "Continuous Phase Equilibrium Data for CO_2 Wasson Line Oil: Supplement to Paper SPE 28974," PRRC Report 95-22, New Mexico Petroleum Recovery Research Center, May 1995, Socorro, NM.
11. Lee, H.O., Heller, J.P., and Hoefer, A.M.W.: "Change in Apparent Viscosity CO_2-Foam with Rock Permeability," *SPERE* (Nov. 1991) 421-428.
12. Tsau, J.-S. and Heller, J.P.: "Evaluation of Surfactants for CO_2-Foam Mobility Control," paper SPE 24013.
13. Chang, S.-H., Owusu, S.B., French, S.B., and Kovarik, F.: "Effect of Microscopic Heterogeneity on CO_2-Foam Mobility: Part 2 - Mechanistic Foam Simulation," paper SPE/DOE 20191 presented at the 7th Symposium on Enhanced Oil Recovery, Tulsa, April 22-25, 1990.
14. Chang, S.-H. and Grigg, R.B.: "Laboratory Flow Tests Used To Determine Reservoir Simulator Foam Parameters for EVGSAU CO_2 Foam Pilot," paper SPE 27675 presented at the 1994 Permian Basin Oil and Gas Recovery Conference, Midland, March 16-18.
15. Heller, J.P., Boone, D.A., and Watts, R.J.: "Tertiary CO_2 Foam for Mobility Control at Rock Creek," paper SPE 14519 presented at the 1985 SPE Regional Conference, Morgantown, Nov. 5-8.

16. Martin, F.D. *et al.*: "CO_2 Foam Field Verification Pilot Test at EVGSAU Injection Project - Phase I: Project Planning and Initial Results," paper SPE/DOE 24176 presented at the 8th Symposium on Enhanced Oil Recovery, Tulsa, April 22-24, 1992.
17. Martin, F.D. *et al.*: "Field Verification of CO_2 Foam," Final Report to the U.S. Department of Energy, April 1995, PRRC Report 95-13 , Petroleum Recovery Research Center, Socorro, NM (March 1995).
18. Peng, D.-Y., and Robinson, D. B.: "A new two-constant equation of state," *Ind. Eng. Chem. Fund.*, 15(1976): 59-64.
19. Riazi, M. R., and Daubert, T. E. : "Characterization parameters for petroleum fractions," *Ind. Eng. Chem. Res.*, 26(1987): 755-759.
20. Whitson, C.H., Anderson, T.F., and Soreide, I.: "C7+ characterization of related equilibrium fluids using the gamma distribution," in Chorn, L. G. and Mansoori, G. A. (eds.), *C7+ Fraction Characterization*. Taylor and Francis, New York, 1989, pp. 35-56.
21. Yarborough, L.: "Application of a generalized equation of state to petroleum reservoir fluids," in Chao, K. C. and Robinson, R. L. Jr. (eds.), *Equation of State in Engineering and Research*. American Chemical Society, Washington, D. C., 1979, pp. 385-439.
22. Chang, S.-H., Grigg, R. B., and Huang, T.-C.: "Characterization and Multiphase Equilibrium Prediction of Crude Oil Heavy Components," International Symposium Thermodynamics of Heavy Oils and Asphaltenes, 1995 AIChE Spring National Meeting, Houston, March 19-23. Accepted for publication in *Fuel Science and Technology International*, in an issue in early 1996.
23. Falls, A.H., Hirasaki, G.J., Patzek, T.W., Gauglitz, D.A., Miller, D.D., and Ratulowski., J.: "Development of a Mechanistic Foam Simulator: The Population Balance and Generation By Snap-Off," *SPERE* (Aug. 1988) 884-892.
24. Friedmann, F., Chen, W.H., and Gauglitz, P.A.: "Experimental and Simulation Study of High-Temperature Foam Displacement in Porous Media," *SPERE* (Feb. 1991) 37-75.
25. Kovseck, A.R., Patzek, T.W., and Radke, C.J.: "Mechanistic Prediction of Foam Displacement in Multidimensions: A Population Balance Approach," paper SPE/DOE 27789, presented at the 1994 SPE/DOE Symposium on Improved Oil Recovery, Tulsa, April 17-20.
26. Stevens, J. E. and Martin, F. D.: "CO_2 Foam Field Verification Pilot Test at EVGSAU: Phase IIIB - Project Operations and Performance Review," paper SPE/DOE 27786, presented at the SPE/DOE Ninth Symposium on Improved Oil Recovery, Tulsa, April 17-20.
27. Babu, D. K., Odeh, A. S. , Al-Khalifa, A. J., and McCann, R. C.: "The Relation Between Wellblock and Wellbore Pressures in Numerical Simulation of Horizontal Wells," *SPERE* (August 1991) 324-328.

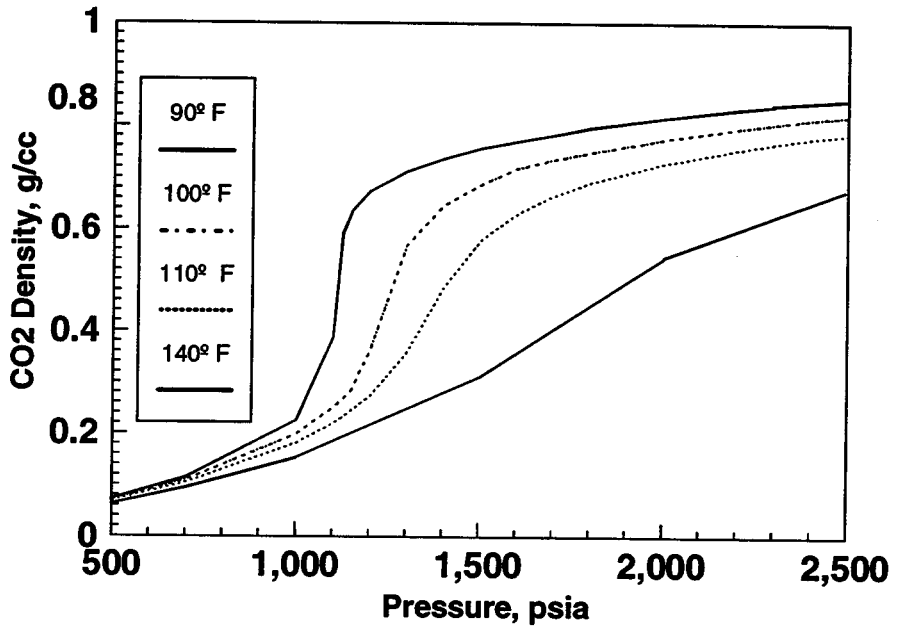

Fig. 2-1. CO_2 density vs temperature and pressure.

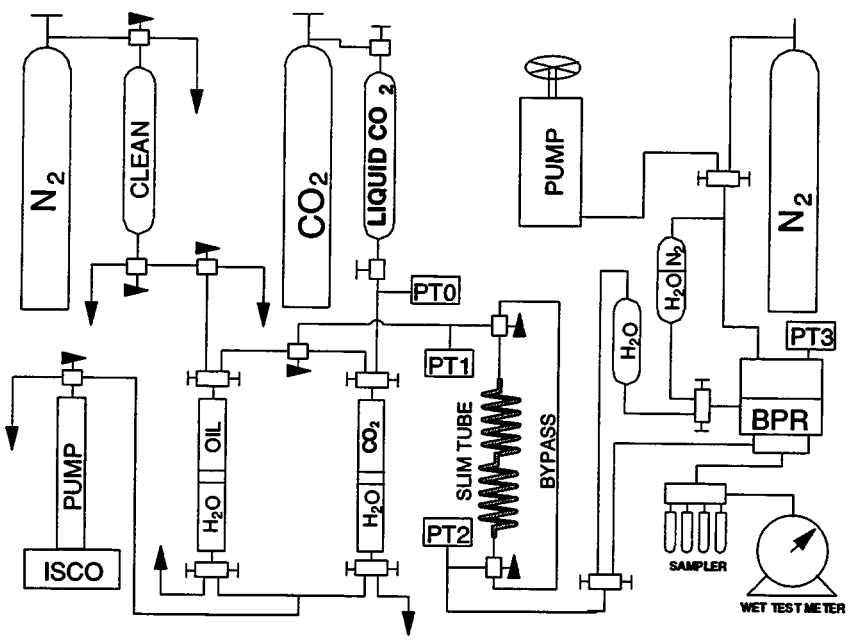

Fig. 2-2. Slim tube apparatus.

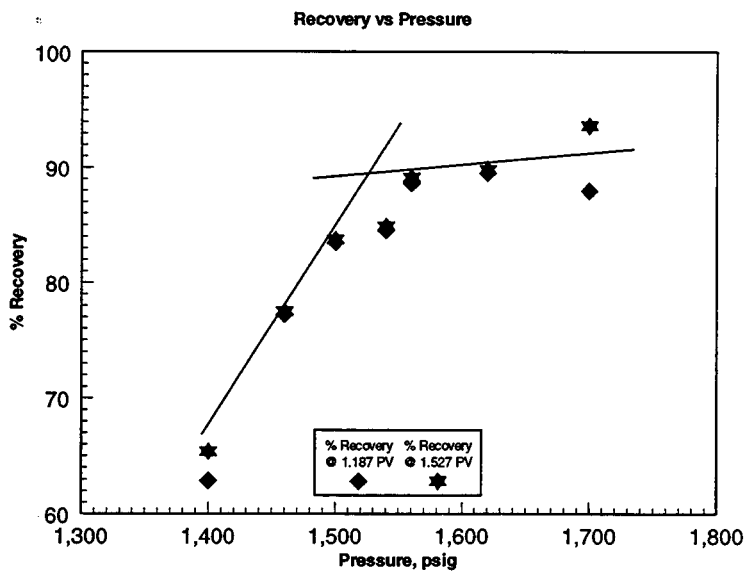

Fig. 2-3. Recovery vs pressure.

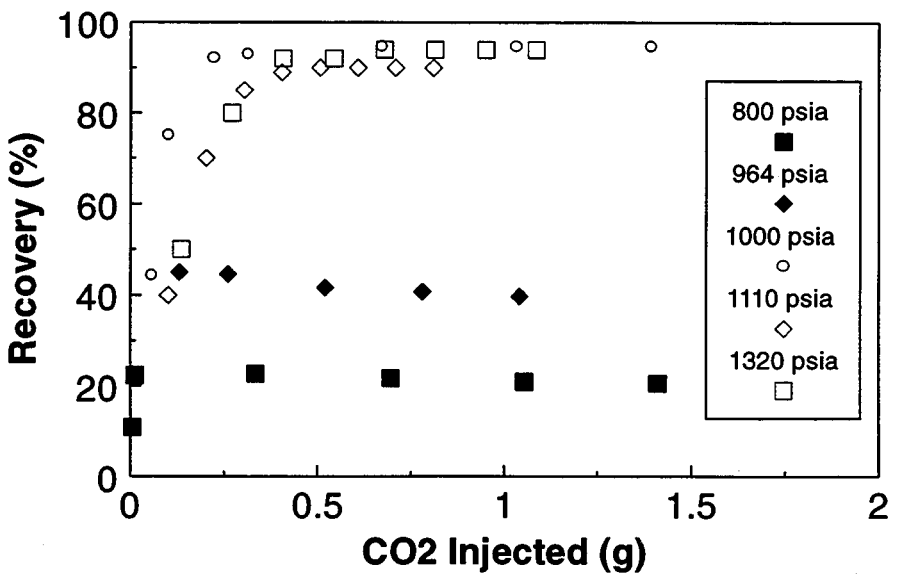

Fig. 2-4. Effect of pressure on sweep efficiency.

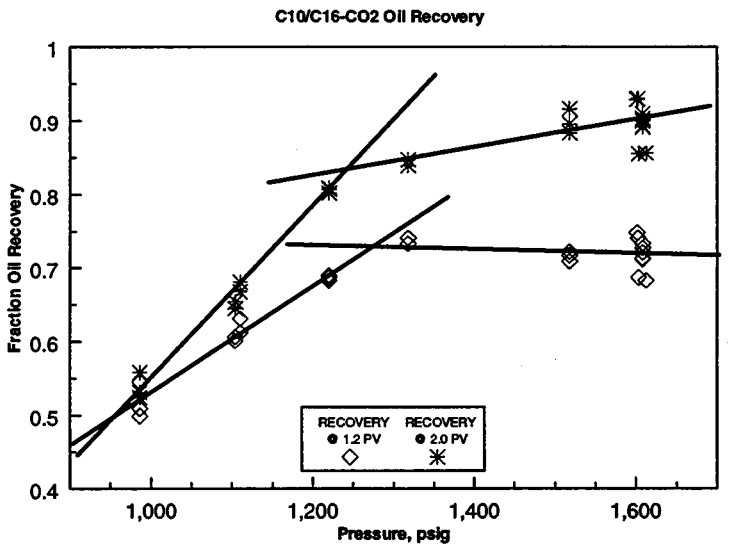

Fig. 2-5. C20-C16-CO_2 oil recovery.

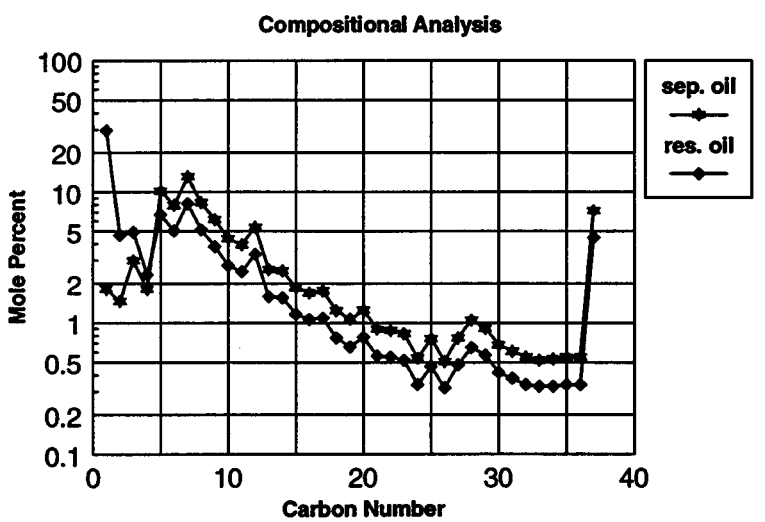

Fig. 2-6. Comparison of the compositions of the separator oil used in the slim tube tests and the recombined oil used in the swelling tests.

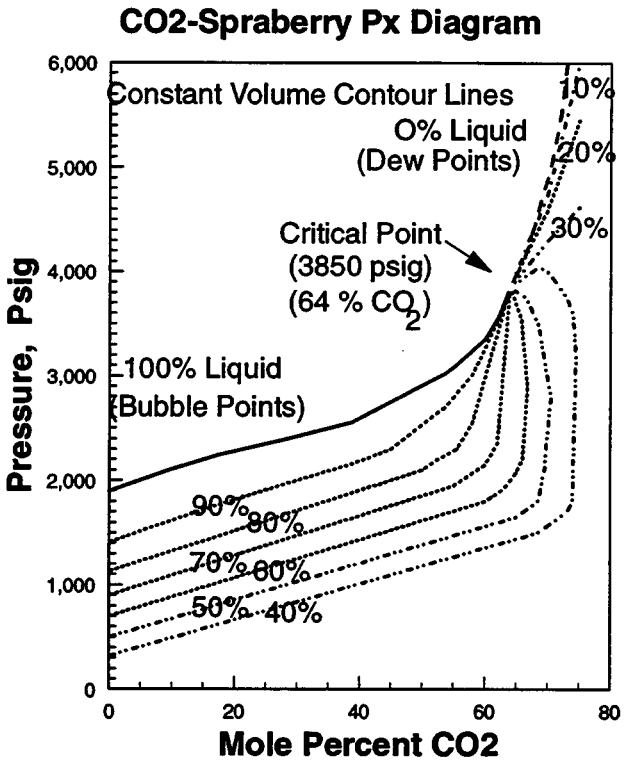

Fig. 2-7. CO_2-Spraberry Px diagram.

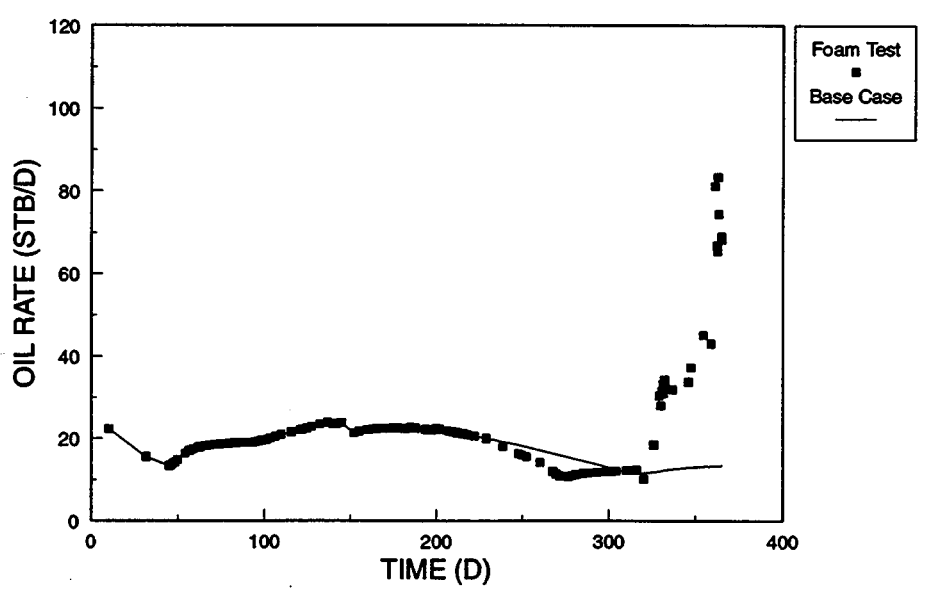

Fig. 2-8. Effect of foam on oil rate.

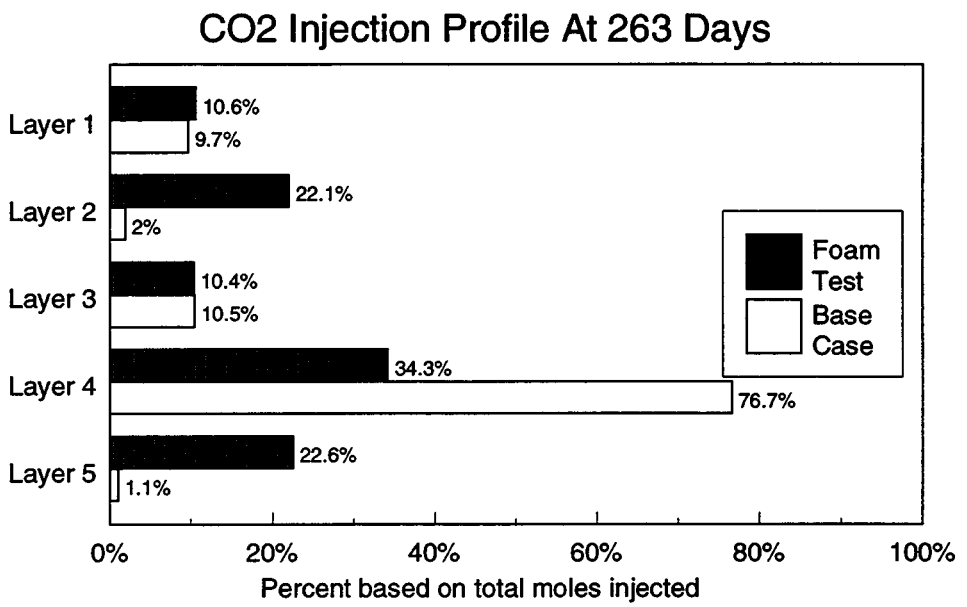

Fig. 2-9. CO_2 injection profile comparison at 263 days of simulation.

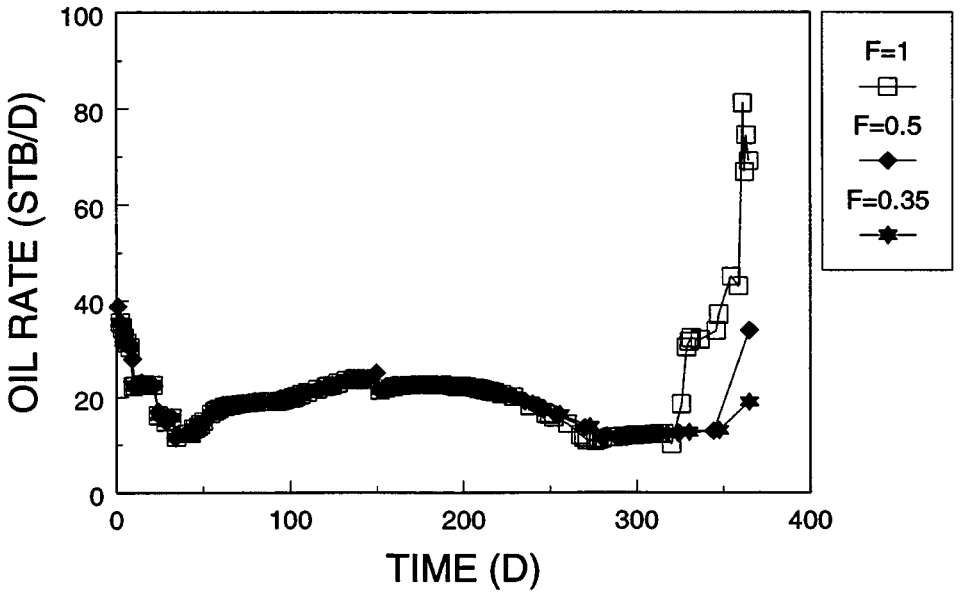

Fig. 2-10. Effect of scaling parameter F on oil rate.

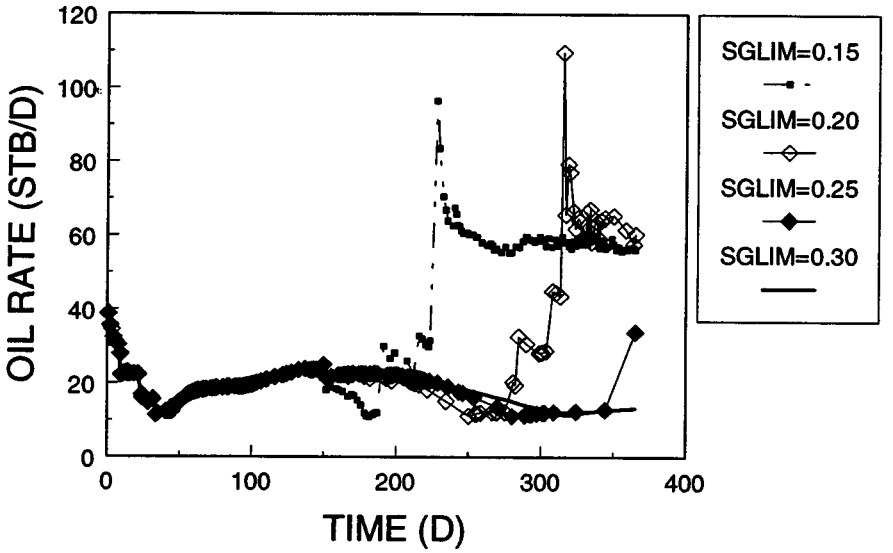

Fig. 2-11. Effect of limiting gas saturation (SGLIM) on oil rate.

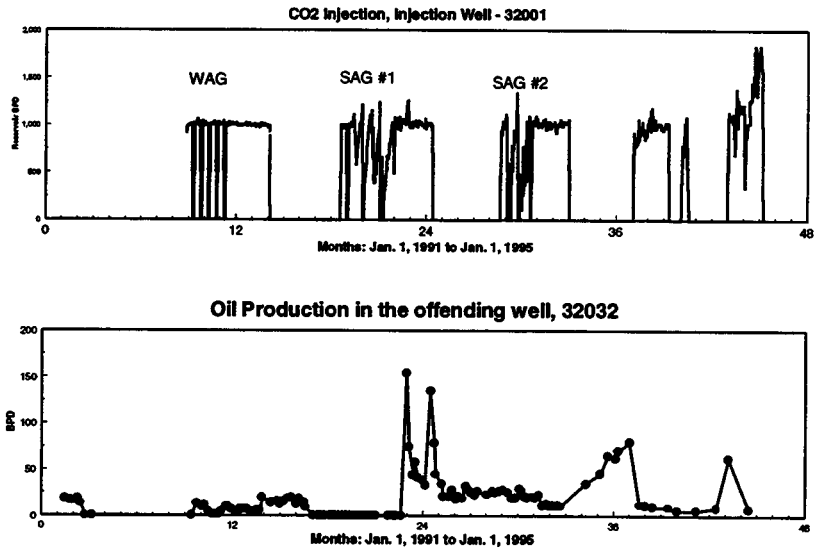

Comparison of Oil Rate to the CO2 injection cycles in Well 32032.

Fig. 2-12. Comparison of oil rate to the CO_2 injection cycles in well 32032.

TASK 3: LOW IFT MECHANISMS WITH APPLICATIONS TO MISCIBLE FLOODING IN FRACTURED RESERVOIRS

INTRODUCTION

The objective of Task 3 primarily concerns facilitating the prediction of interfacial tension (IFT) calculations used in all aspects of reservoir engineering, particularly gas injection processes and gas condensate reservoirs. Accomplishment of Task 3 would provide reservoir engineers with a reliable tool for predicting IFT under a wide range of reservoir conditions. Of particular interest are low and high values of gas/oil IFT, gas/brine IFT at reservoir conditions, and oil/brine IFT at reservoir conditions.

There is no systematic method for calculation of any of the above stated systems. We have found considerable confusion in the literature, even for the calculation of simple gas/oil systems via the parachor method. As a result, we have rigorously investigated both the origin and evolution of the methodologies developed for IFT prediction. Here is a summary of the results of our research into IFT predictions:

1) Many past methodologies were developed with implicit, and incorrect, assumptions regarding the scaling exponent between IFT and density difference which is the key to parachor calculations.

2) Recent theoretical research in the physics literature appears to have isolated and verified the scaling exponents yet the petroleum industry has been unaware of the advances.

3) We have investigated scaling behavior near and far from the critical point and found that the scaling exponents are unique, therefore should not be used as adjustable parameters.

4) Parachors for pure components and C_{7+} fractions have been recalculated from carefully selected data found in over 250 technical papers. The parachors are based on current understanding of critical phenomena, thus they too should not be used as adjustable parameters.

5) The modified parachor method presented in this report has proven superior to other parachor calculations for application in low and high IFT systems, both CO_2/oil and gas-condensates.

STATUS OF PENDANT DROP APPARATUS

Verification of IFT for calculations at reservoir conditons is essential to validate our gas-oil parachor methodology and future development of a reliable tool for estimating IFT in brine/crude and

brine/gas systems. We have embarked upon development of a pendant drop apparatus to measure a wide range of IFT for all three systems of interest.

Construction of the system is complete. We are able to circulate fluids and form drops through a variety of needle bore sizes. Densities of equilibrated phases can be measured by circulating through a densitometer. We have tested low IFT alcohol/oil/water systems at low pressure. We are able to form drops at low IFT, although we have encountered video imaging problems. The primary problem is the ability for our current frame grabber and digitizer to capture a sharp edge for the entire drop. The contrast between the drop and background is obviously less-pronounced at low IFT so we are trying several different methods to improve the contrast. An example of a drop captured by our imaging software is shown in Fig. 3-1.

At the same time, we are adapting commercial code to analyze the image in order to meet our specific system requirements. We are currently pressure testing our measurement cell to delineate the upper limit of our experimental ability. We have sucessfully pressure tested the pendant drop vessel to 2000 psi. The next step involves working with simple, well-described systems in preparation for reservoir fluid/condition measurements in the future.

INVESTIGATION ON PARACHOR METHOD FOR IFT PREDICTION

Background

IFT is one of the key parameters controlling recovery from oil reservoirs. In a low IFT region that occurs around the critical point close to dew and bubble point lines, the IFT dominates relative permeabilities and residual liquid saturations. Prediction of IFT is essential for modeling many secondary and tertiary oil recovery processes. However, there is no consistent standard by which this may be accomplished.

Prediction of the IFT of multicomponent systems using thermodynamics of adsorption at the interface has been demonstrated by Guggenheim and Adam[1] at low pressures where the vapor density is negligibly small. The commonly used methods in the petroleum industry for predicting IFT are empirical correlations called Parachor Methods because of their simplicity. Although recently, the gradient theory has been demonstrated to be superior to the parachor method, it may be applied accurately to interfaces at only conditions far from the critical region according to Cornelisse *et al.*[2] We are interested in calculations of IFT of reservoir fluids, both in the low and high IFT regions. Therefore, only Parachor Methods are discussed in this paper. Based on experimental observations, Macleod[3] recognized the following relation between surface tension and densities:

$$\frac{\sigma}{(\rho_1 - \rho_v)^4} = C \qquad (1)$$

where σ is surface tension, ρ_l and ρ_v are densities of the liquid and vapor phases, respectively, and C is a constant. The exponent 4 was adopted from Van der Waal's equation, which is based on the assumption that the force of attraction between molecules falls off as the 4th power of distance between them. Sugden[3] related the constant C to chemical composition of the substance. He defined a parameter by

$$P = \frac{M}{\rho_l - \rho_v} \sigma^{\frac{1}{4}} \tag{2}$$

where M is molecular weight and P is called *parachor,* which was believed to be a measure of the molecular volume and chemical composition. After Sugden's definition of the parachor in 1924, many researchers have interpreted and evaluated parachors for a variety of pure substances. Quayle[5] provides a summary of these investigations.

The parachors had been limited to calculations of surface tensions of pure substances until the 1940s when the concept was introduced to petroleum industry. Weinaug and Katz[6] employed the pure substance parachors to calculate the IFT of mixtures; Katz *et al.*[7] utilized the parachors to determine the IFT of crude oils; and Reno and Katz[8] tried to determine the IFT of hydrocarbons containing dissolved nitrogen. The equation they used for the multicomponent systems is essentially a linear combination of equations for pure substances with mole fraction weighting:

$$\sigma = \left[\sum_{i=1}^{n} P_i \left(x_i \frac{\rho_l}{M_l} - y_i \frac{\rho_v}{M_v} \right) \right]^4 \tag{3}$$

where x_i and y_i are mole fractions of component i in liquid phase and vapor phase, respectively. Based on experimental observations for propane and normal butane, Hough and Stegemeier[9] proposed the following equation for mixture IFT calculations:

$$\sigma = \left[\sum_{i=1}^{n} P_i \left(\frac{x_i}{V_l} - \frac{y_i}{V_v} \right) \right]^{3.67} \tag{4}$$

where V_l and V_v are molar volumes of liquid phase and vapor phase, respectively. Equation (4) is identical to Eq. (3) with the only difference of scaling exponent 3.67 rather than 4. Lee and Chien[10] also presented an equation for mixture IFT calculations:

$$\sigma = \left[\sum_{i=1}^{n} P_i \left(x_i \frac{\rho_l}{M_l} - y_i \frac{\rho_v}{M_v} \right) \right]^{3.91} \tag{5}$$

According to Lee and Chien, the parachor can be determined based on critical properties of the components. A slight modification to the Weinaug-Katz equation was made by Hugill and Van Welsenes[11] using a correlation for pure component parachors and a two-parameter mixing rule for mixture parachors.

Firoozabadi *et al.*[12] compared calculated surface tensions of reservoir crude oil/gas systems using the Weinaug-Katz method with experimental data and claimed that for reservoir-fluid systems that do not contain asphalt materials, a quadratic parachor correlation would suffice for computation of interfacial tension. Gasem *et al.*[13] tested the prediction methods proposed by Weinaug and Katz, the modifications by Hugill and Van Welsenes, and Lee and Chien for IFT of CO_2 and ethane in hydrocarbon solvents. They concluded that the Weinaug-Katz method gives IFT results with an average error of less than 10% when a scaling exponent of 3.66, instead of 4, is used. Many linear and non-linear correlations for parachors have been developed since 1936. Ali[14] compared these parachor methods and modifications using ten parachor correlations. He concluded that the Weinaug-Katz method with a linear parachor correlation that appears in Fanchi[15] yields the best IFT predictions for reservoir oil/gas systems with a mean absolute deviation of 22.2%. Ali also showed that Lee-Chien method can produce large errors in reservoir fluid calculations where the critical properties of the heavy fluid components are uncertain. Based on statistical analysis, Fawcett[16] evaluated correlations and parachors to predict low IFT in condensate systems. He concluded that the Hough-Stegemeier method with a linear correlation for crude cut parachors gives low IFT predictions with small systematic errors for multicomponent systems.

Obviously there has been considerable confusion in the literature concerning the parachor method for estimating IFT. The confusion is primarily based upon the lack of precise definition of the scaling exponent and parachors derived based on this exponent. This paper addresses: (1) clarification of the confusion about the scaling exponent, (2) derivation of parachors for pure species occurring in petroleum fluids and oil cuts, and (3) verification of the validity of these derived parachors in IFT prediction of reservoir fluids.

Scaling Exponent

This section discusses the origin of various values of the scaling exponent that appear in the literature. The applicability of the scaling exponent 3.88 established in the modern physics literature is evaluated using experimental data for 23 compounds and compound mixtures occurring in petroleum fluids.

Origin of Various Values

From the last section, the exponent 4 in the Weinaug-Katz equation (Eq. 3) was adopted, through Macleod and Sugden, from the Van der Waal's equation without any justification. Macleod assumed that since the Van der Waal's equation is based on the assumption that the force of attraction between molecules falls off as the 4th power of distance between them, then the value 4 should be the scaling exponent. We have re-examined Macleod's original data and found this exponent 4 to be a rough approximation. The actual values of Macleod's exponent are less than 4 as shown in Fig. 3-2 and Table 3-1.

Another means of quantifying the exponent is to use the critical scaling theory for IFT:

$$\sigma = \sigma_0 \left(l - \frac{T}{T_c} \right)^{\gamma} , \tag{6}$$

and density difference:

$$\Delta\rho = \Delta\rho_0 \left(1 - \frac{T}{T_c} \right)^{\beta} \tag{7}$$

Dividing Eq. (6) by Eq. (7) gives a relationship between IFT and $\Delta\rho$. The constant C is related to

$$\sigma = C(\Delta\rho)^{\frac{\gamma}{\beta}} \tag{8}$$

parachor and the ratio of the two critical scaling exponents, $\frac{\gamma}{\beta}$, is equivalent to the exponent in the parachor equation.

Based on empirical relations given by Guggenheim,[17] Hough and Stegemier[9] proposed values of 1/3 (or 0.33) for $\Delta\rho$ and 11/9 (or 1.22) for γ. The ratio of these two values gives Hough-Stegemeier's scaling exponent of 11/3 (or 3.67). The empirical relations provided by Guggenheim originally appeared in Guggenheim's early work[18] published in 1945. These relations were established based on limited measurement of $\Delta\rho$ and IFT. The eight fluids used were *Ne, Ar, Kr, Xe,* N_2, O_2, *CO*, and CH_4.

At one time, many researchers believed that all materials have the same β exponent 1/3. However, until the 1970s, this had not been rigorously demonstrated as pointed out by Stanley.[19] It can be seen that the 1/3 proposed by Guggenheim had not been accepted by physicists as a general

value for β when it was adopted by Hough and Stegemeier. The γ value 11/9 was also established by Guggenheim's work[17] based on limited measurements on *Ne, Ar,* N_2 and O_2. Again, the scaling exponent 11/9 had not been accepted in the physics literature as a general value for β when it was adopted by Hough and Stegemeier in 1961. Therefore, it appears that the exponent 3.67 proposed by Hough and Stegemeier is not applicable to all fluids. Lee and Chien[10] adopted β and γ values from different sources. They used the empirical value 11/9 (or 1.22) for γ given by Guggenheim[17] and theoretical value 0.3125 for β given by Fisher.[20] The ratio of these two values gives Lee-Chien's scaling exponent of 3.91. The 0.3125 is based on one of a class of decorated Ising models described by Fisher.[21] According to this model, the γ value is 1.25 rather than 1.22. This reveals that the scaling exponent 3.91 in Lee-Chien's equation may not be reliable because it was established based on inconsistent data sources.

Sengers and Sengers[22] summarized theoretical values of these critical scaling exponents found in the physics literature as shown in Table 3-2. According to Ising, model series expansions β and γ have theoretical values of 0.312 and 1.25, respectively. The ratio between them is 4. Based on renormalization group theory, the β and γ have theoretical values of 0.325 and 1.241, respectively. The ratio between them is 3.82. The currently accepted values for β and γ in modern physics are 0.325 and 1.26, respectively (Rowlinson and Widom,[23] Widom,[24] and Moldover[25]) yielding 3.88 for the critical scaling exponent in the parachor equation.

Applicability of Exponent 3.88

The question of applicability of critical scaling exponents well away from the critical point has been speculated upon, but no evidence can be found in the literature which proves or disproves the extent of critical scaling and what governs deviations from critical scaling far from the critical point. From Macleod's data shown in Fig. 3-2, we could assume that the theoretically derived critical exponent (3.88) may be applicable over a wide range of conditions, while other more recent papers have suggested this number should be altered away from the critical region.

Haniff and Pearce[26] discussed the four exponents (4, 3.67, 3.91 and 3.88) that appear in parachor equations. They also measured IFT and $\Delta\rho$ of C_1/C_3 mixtures at different temperatures. By fitting their experimental data to the parachor equation, they found that the exponent in the parachor equation increases with temperature. This exponent increases from 3.70 to 3.83 as temperature increases from 29.6° C to 39.2° C for the C_1/C_3 mixture. Since all these values are less than 3.88, they believed that the experimental points were outside the critical region. They also considered the value 3.70, which was derived at a temperature of 29.6°C, to correspond to Hough-Stegemier's exponent 3.67. They concluded that along the critical isotherm and, more particularly, in the vary narrow region close to the critical point, the exponent is equal to 3.88. They referred to exponent values that are less than 3.88 as "effective" critical exponents. Huygens et al.[27] plotted IFT-density data taken from studies by Haniff and Pearce,[26] Wagner and Leach,[28] Firoozabadi and Ramey,[29] and Satherley *et al.* [30] in one graph. They found that when all the data points are considered in a wide range of IFT below 1 mN/m, the data exhibits a linear relationship on a log-log scale with a slope of 3.88 which is consistent with the theoretical value of the scaling exponent.

Accordingly, they define the critical region as the region where the IFT is less than 1 mN/m.

To explore the applicability of the scaling exponent 3.88, we first plotted IFT versus reduced temperature ($1-T/T_c$) data in the low IFT region for methyl ether and CO_2 as demonstrated in Fig. 3-3. The slope is very close to 1.26. We then plotted IFT versus reduced temperature ($1-T/T_c$) data for 57 pure components. Data are cited from Vargaftik.[31] The measured IFT data are mostly between 10 mN/m and 30 mN/m. IFT was measured at reduced temperatures mostly ranging from 0.2 to 0.6. Although most of data points fall far beyond the critical region defined by Huygens et al., distribution analysis shown in Fig. 3-4 indicates that most of the slope values are still in the neighborhood of 1.25 which is close to the critical scaling exponent 1.26.

Figure 3-5 shows a plot of density difference versus reduced temperature for the iso-butyric acid/water system studied by Greer.[32] This figure demonstrates the validity of the scaling exponent $\beta = 0.325$ near to the critical point. While similar data are lacking in literature, more IFT-density data for multicomponent mixtures are available from previous investigations. Figure 3-6 shows a plot of IFT vs. $\Delta\rho$ for methane-propane mixtures at various temperatures. Data used to generate this plot are from Weinaug and Katz's[6] paper for the C_1/C_3 binary system. The experimental data conforms closely to the slope derived by critical scaling theory, even well away from what is considered "near critical". This figure indicates that for this gas condensate system the slope of 3.88 holds at least up to an IFT value of 10 mN/m. Figure 3-7 shows experimental data presented by Satherley *et al.*,[33] Morrow *et al.*,[34] and Cuiec *et al.*[35] for oil/brine systems containing alcohol. This figure tends to confirm Huygens *et al.* definition of the near-critical region. Shown in Fig. 3-8 are data obtained by Huygens *et al.* and Satherley and Schiffrin for three nitrogen/hydrocarbon systems. This figure indicates that the near-critical region for the nitrogen/hydrocarbon systems may be much narrower than that defined by Huygens *et al.* The slope drops below 3.88 when the IFT is greater than 0.1 mN/m. Figure 3-9 shows experimental data provided by Hsu *et al.*,[36] Nagarajan and Robinson,[37,38] and Gasem et al.[39,40] for some CO_2 hydrocarbon systems. The experimental data match the slope derived by critical scaling theory closely, even well away (IFTs up to 10 mN/m) from what is considered "near critical" except for the C_{14}/CO_2 system which has a relatively narrow critical region.

It must be emphasized that near the critical point, the slope has a theoretical value of 3.88 regardless of the path taken to the critical point, whether by change in temperature or pressure (as in the case of CO_2-hydrocarbon mixtures) or adding a third component such as alcohol. Figures 3-2 and 3-6 through 3-9 clearly demonstrate that as low IFT values are achieved (approximately below 1.0 dyne/cm), the slope of the plot is very near the theoretical value of 3.88. It has been shown in Figs. 3-7 and 3-8 that alcohol/oil/water and N_2/hydrocarbon systems deviate from a slope of 3.88 at higher values of IFT. The deviation of the nitrogen/hydrocarbon and alcohol/oil/water systems from critical exponents are explained by the following: If a single drop of alcohol is added to an oil/water system, the alcohol will rapidly adsorb at the interface. The IFT will be significantly reduced yet the density difference between the bulk phases will change very little. The result is that the slope of the IFT/$\Delta\rho$ plot is greater than 3.88. Conversely, nitrogen weakly adsorbs at the interface, thereby requiring high pressures for significant solubility and mass transfer between the phases before

the IFT is lowered. In addition, the molecular weight of nitrogen is lower than that of most hydrocarbons in oil, therefore, it usually has a negative contribution to gas density, which keeps IFT high. Thus, the nitrogen/hydrocarbon slopes are seen to be less than 3.88. These special systems are discussed in a separate section in this paper.

In summary, for strongly interacting systems, *e.g.*, brine/oil/alcohol, weakly interacting systems, *e.g.*, N_2/oil, or molecules with a large size discrepancy, *e.g.*, CO_2/C_{14}, the scaling exponent may not be valid outside the critical region as defined by Huygens *et al.* However, for CO_2, crude, or gas condensate systems, the scaling exponent's wide range of validity ensures relatively accurate IFT predictions by the parachor method.

New Parachors

This section presents parachors of pure components derived using 3.88 as the scaling exponent. These parachors are correlated to molecular weight. Correlations have been developed for hydrocarbon mixtures with different composition. Parachors of oil cuts are determined utilizing these correlations.

Pure Substance

Parachors of CO_2, N_2, H_2S and 136 hydrocarbons commonly encountered in crude oils are back calculated from measured density and interfacial tension data. The experimental data are obtained from references 3, 4, 5, and 41 through 72. These experimental data are carefully screened from 259 technical papers. Experimental data consistently provided by different investigators are selected for parachor determinations in this work. The resultant parachors are presented in Table 3-3. With some mixing rule, these parachor data can be utilized for predicting IFT of well defined hydrocarbon systems with known exact compositions.

Hydrocarbon Mixtures

It is convenient to lump, sometimes split, hydrocarbon components in analyzing hydrocarbon "plus fractions" of crude oil systems. Usually, the plus fractions, commonly known as the C_{7+} fractions, contain an indefinite number of components with a carbon number higher than six. Molecular weight and specific gravity of the C_{7+} fraction may be the only measured data available. Therefore, it is desirable to assign parachors to the plus fractions based on the molecular weights. We have plotted molecular weight vs. parachor data for different hydrocarbon mixtures as shown in Figs. 3-10 through 3-15. These figures indicate that there exists a fairly good linear relationship for a variety of hydrocarbons. This linear relationship can be expressed as

$$P = a\,M + b. \qquad \textbf{(9)}$$

Correlation coefficients and standard error of estimation for these hydrocarbons are summarized in Table 3-4. It is evident from Table 3-4 that normal paraffins remarkably obey the

linearity, while adding cyclic and aromatic compounds causes scatter of data. It is recommended that these correlations be used for estimating parachors of the plus fractions. One of the correlations should be chosen based on an estimation of the composition of the plus fraction. The estimation may be made through PONA (paraffin/olefin/naphthene/aromatic) analysis of stock-tank-oil.

Parachors of Oil Cuts

Although it is possible to get reliable parachors for pure components, the applications of pure component parachors are limited to simple fluid systems with known exact compositions. This is particularly true in petroleum reservoir simulation where hydrocarbons are treated in their groups (oil cuts). For example, group C_6 includes normal hexane, 2-methylpentane, 3-methylpentane, 2,2-dimethylbutane, 2,3-dimethylbutane, etc. With currently available technologies, it is difficult, if not impossible, to measure the exact composition of a crude oil. Also, it is not feasible to simulate crude oil systems using all the exact components. Even if this could be done, physical properties, such as critical pressure, of all the pure components are not readily available. Therefore, it is desirable to assign parachors to hydrocarbon groups (oil cuts) for uses in compositional reservoir simulators. Based on equivalent molecular weights of oil cuts proposed by Ahmed,[73] parachors of hydrocarbon groups are estimated using a linear correlation. The results are shown in Table 3-5.

Comparisons

Several parachor correlations have been reported to be successful for predicting IFT of reservoir fluids. Firoozabadi *et al.*[12] claimed that for reservoir-fluid systems that do not contain asphalt materials, the following quadratic parachor correlation would suffice for the computation of surface tension when Weinaug-Katz parachor method is used:

$$P = -11.4 + 3.23\,M - 0.0022\,M^2. \qquad \textbf{(10)}$$

Through comparison of ten parachor correlations, Ali[14] concluded that the linear parachor correlation that appears in Fanchi (1990) best fits the Weinaug-Katz parachor method and yields the least error in IFT predictions. The linear parachor correlation is given by

$$P = 69.9 + 2.3\,M. \qquad \textbf{(11)}$$

Fawcett[16] claimed that the Hough-Stegemeier method gives good IFT predictions if the following linear correlation for crude cut parachors is employed:

$$P = 81.2 + 2.448\,M. \qquad \textbf{(12)}$$

In this section, measured IFTs of 6 reservoir oil/CO_2 mixtures are compared with the IFTs predicted by Peng-Robinson equation of state (PREOS) using the following approaches:

A. Use scaling exponent 4 and Eq. (10)
B. Use scaling exponent 4 and Eq. (11)
C. Use scaling exponent 3.67 and Eq. (12)
D. Use scaling exponent 3.88 and Eq. (9)

The last approach is proposed by this work. The Lee-Chien method is not compared here because of uncertainties involved in determination of critical properties of heavy components.

The six reservoir oil/CO_2 systems with given IFT measurements are

I. Asphalt-free oil used by Firoozabadi *et al.*[11]
II. Oil A used by Firoozabadi *et al.*[11]
III Oil C used by Firoozabadi *et al.*[11]
IV. Oil D used by Firoozabadi *et al.*[11]
V. Oil A plus 55% CO_2 used by Simon *et al.*[74]
VI. Recombined Oil plus 55.55% CO_2 used by Gasem *et al.*[40]

Measured compositions and characterizations of C_{7+} of these reservoir oils, and experimental temperatures when IFTs were measured, are summarized in Table 3-6.

Using the PREOS and the four approaches, the IFT of six reservoir oil/CO_2 mixtures at different pressures is predicted. For the first five fluid systems, the predicted IFT data are compared with measured IFT data in Table 3-7. When Approach D was used, the last set of correlation coefficients in Table 3-4 was employed. Table 3-7 indicates that Approach D yields the least error in IFT predictions. The predicted and measured IFT data for System VI are compared in Fig. 3-16. This figure again shows that Approach D allows better prediction of IFT compared to other approaches, especially in the near critical region.

As an example of the application of Approach D, we have computed IFT for mixtures of CO_2 and oil from the Spraberry Trend Area in West Texas. Equi-IFT maps are generated for modeling fluid flow in the reservoir. These maps are shown in Figs. 3-17 and 3-18 for CO_2 stock tank oil and CO_2/recombined reservoir oil, respectively. This figure also demonstrates the range of convergence for density calculations via the PREOS.

Discussion of Scaling Exponent

This section presents our arguments about the treatment of the scaling exponent, parachor, and special systems that do not obey the scaling law under conditions normally encountered in petroleum reservoirs. From recent work such as Danesh *et al.*,[75] researchers have proposed the critical scaling exponent in the parachor equation is a function of density difference. They used the

critical scaling exponent as an adjustable parameter to fit the experimental data. We think this is not a theoretically correct approach. The critical scaling exponent has a unique value in what is typically considered the critical region. Many parachor values found in the literature were derived based on constant scaling exponents (mostly 4). If a constant parachor and varying exponents are utilized, the inconsistency will result in inaccurate IFT predictions of unknown systems. We believe that outside the critical region, where the critical scaling exponent 3.88 is not valid, correlations such as the one proposed by Firoozabadi and Ramey[29] should be developed for IFT predictions. Also adsorption theory may be suitable for IFT calculations in such cases.

Parachors

Reno and Katz[8] measured IFT of normal heptane and normal butane containing dissolved nitrogen at different pressure and temperatures. They calculated IFT using the parachor method presented by Eq. (3). The calculated IFT data match the measured IFT data only when the parachor of nitrogen in the mixture is adjusted from pure nitrogen parachor of 60 to 41. Huygens *et al.*[27] measured the IFT of four hydrocarbon mixtures containing nitrogen. They found that Eq. (4) fails to predict IFT of the nitrogen/hydrocarbon systems if the parachor of pure nitrogen is used. In order to match the measured IFT, they had to vary nitrogen parachor for different mixtures. Since parachor is a property of the pure component, we argue that each component should have its unique parachor no matter whether the component exists in its pure state or in mixtures with other substances. We believe that varying the parachor for a given component is not consistent with critical scaling.

Special Systems

Systems like brine/alcohol/oil, N_2/hydrocarbon, and CO_2/C_{14} are considered special systems because the critical region, where critical scaling theory is valid, is narrow. These systems are strongly interacting, weakly interacting, or molecules with a large size discrepancy. Since the parachor method fails to predict the IFT of these systems under conditions that normally occur for petroleum fluids, the IFT can be better predicted using adsorption theory.

We have re-calculated the IFT of the nitrogen/hydrocarbon systems that were investigated by Reno and Katz[8] and Huygens *et al.*[27] using new parachors. We confirmed the observations by the above researchers: the parachor method does not work well for some hydrocarbon systems containing dissolved nitrogen if the pure nitrogen parachor is used. We speculate that the parachor method for mixtures represented by Eqs. (3), (4) and (5) is an approximation extended from the parachor method for pure substance using a linear mixing rule. Although it works well for some hydrocarbon and CO_2/hydrocarbon mixtures, it is not generally applicable to all mixtures, such as nitrogen/hydrocarbon mixtures that behave very differently from hydrocarbon compounds due to their different chemical properties, adsorption and solubility behavior.

To support our argument, let us examine Eq. (3) carefully. This equation was proposed by Weinaug and Katz[6] based on equations derived by Sugden[4] and Fowler[76] for pure substances. When this equation was formed, it was assumed that the parachor is a linear, additive, and constitutive

property, which may not be true for all mixtures, especially nitrogen and hydrocarbons that are chemically very different. Also, it was conceived by Weinaug and Katz that a method of applying mole fraction of each constituent in its respective phase to molal volumes of phases is valid. It was expected that each constituent contributes a positive IFT component to the total IFT of the system. However, we have found that the term $x_i\frac{\rho_l}{M_l} - y_i\frac{\rho_v}{M_v}$ in Eq. (3) could be negative for some gaseous constituents such as nitrogen. This is mainly because y_i is significantly higher than x_i for these constituents and M_v is significantly lower than M_l in the system. When these terms are negative, negative contributions of these constituents to the IFT of the mixture are calculated, which physically makes no sense.

This argument can also be justified by considering the adsorption mechanism. Chemical properties of a component of a mixture govern adsorption of the component at the liquid-vapor interface of the system. Consider two systems: the first one is a propane/IPA (2-propanol) mixture, and the second one is propane containing dissolved nitrogen. To compare the two systems, let us define relative interface adsorption, I_l and I_v, for component i as

$$I_i = \frac{x_i^s}{x_i} \tag{13}$$

and

$$I_i = \frac{x_i^s}{x_i} \tag{14}$$

where x_i^s is mole fraction of component i at the liquid-vapor interface. By these definitions, l_i and l_v reflect the relative amount of a component adsorbed at the two-phase interface compared to that in each phase. The x_i^s for the two systems at different pressures are computed. Equations derived for the computation are to be presented in a separate paper. The result of the computation shows that the mole fraction of the IPA at the interface is high compared to that in the vapor phase $(I_v > 1)$, and it increases quickly with elevated pressure. However, the mole fraction of the IPA at the two-phase interface is almost the same as that in the liquid phase, $(I_v \approx 1)$ and it is not sensitive to pressure. This indicates that IPA in the vapor phase is favorable to be adsorbed at the interface, and pressure helps this adsorption. This is expected because IPA is a surfactant which reduces interfacial tension by active adsorption at the interface. From this point of view, it is anticipated that the IFT of mixtures containing IPA should decrease rapidly with increased pressure.

The result of the computation also shows that the mole fraction of the nitrogen at the two-phase interface is low compared to that in the vapor phase ($I_v > 1$), and it increases slowly with elevated pressure. However, the mole fraction of the nitrogen at the two-phase interface is higher than that in the liquid phase ($I_v \approx 1$), and it decreases slowly when pressure is increased. This indicates that nitrogen in the vapor phase is neither favorable to be adsorbed at the interface nor favorable to be dissolved in the liquid phase, and pressure does not effectively help the adsorption or the solubility of the nitrogen. In other words, nitrogen is not surface-active. Based on this reasoning, it is anticipated that the IFT of mixtures containing much nitrogen should not decrease rapidly with increased pressure in some pressure range. This is consistent with experimental data (Fig. 3-8) showing slow decline of IFT of N_2/toluene and $N_2/n\text{-}C_{14}$ systems outside of the critical region as pressure increases.

It is concluded from the above analysis that the adsorption behavior of nitrogen is very different from the adsorption behavior of IPA at the liquid/vapor interface. Since the adsorption mechanism governs IFT of the system through surface excess, it is necessary to analyze the IFT of nitrogen/hydrocarbon or alcohol/oil/brine systems using adsorption theory.

CONCLUSIONS

1. According to current understanding in the physics literature, the critical scaling exponent in the parachor equation is 3.88.

2. The scaling exponent and parachors calculated based on critical scaling should not be used as adjustable parameters in prediction of multicomponent IFT.

3. Based on the exponent 3.88, new parachors of pure substances commonly encountered in petroleum fluids are obtained from carefully selected density and surface tension data. The parachors of hydrocarbon mixtures are linearly correlated to their molecular weights. Normal paraffins remarkably obey the linearity, while adding cyclic and aromatic compounds to the mixture causes scatter of data. Parachors of hydrocarbon groups (oil cuts) are assigned to their equivalent molecular weights using a linear correlation.

4. These newly developed pure component parachors, parachor correlations, and oil cut parachors are tested for IFT predictions using six reservoir oil/CO_2 mixtures. These tests indicate that the new parachors and correlations are better than those proposed by previous investigators in terms of IFT predictions of reservoir fluids. When the parachor method and the new parachors and correlations are employed, IFT of reservoir fluids can be predicted using Peng-Robinson equation of state with an acceptable error.

5. The parachor method works well combined with the PREOS for CO_2/crude and gas condensates yet fails to predict IFT of some special systems such as nitrogen/hydrocarbon mixtures. Future research work should include analysis of IFT of such special mixtures using adsorption theory.

COMPLEMENTARY RESEARCH AND FIELD APPLICATIONS

We are currently awaiting final approval of a Class III DOE funded Program Opportunity Notice (PON). The PRRC has teamed with Parker and Parsley of Midland, TX, to test the feasibility of CO_2 injection in naturally fractured Spraberry Trend Area in a 16 well pilot pattern.

Prediction of IFT between Spraberry crude and CO_2 is an important element to understanding fluid flow in the reservoir. We are also concerned with modeling low IFT gravity drainage and our experiments in this area are dependent upon accurate knowledge of low IFT gas/oil systems.

We have developed a new model describing low IFT gravity drainage which will be reported in the upcoming quarter.

Nomenclature

a	=	correlation coefficient
b	=	correlation coefficient
C	=	constant in Macleod Equation
I	=	relative adsorption index
M	=	molecular weight
n	=	number of components
P	=	parachor
T	=	temperature, absolute, degree centigrade
V	=	molar volume, L^3, cm^3
x	=	mole fraction in liquid phase
y	=	mole fraction in vapor phase
ρ	=	phase density, m/L^3, $gram/cm^3$
$\Delta\rho$	=	density difference, m/L^3, $gram/cm^3$
β	=	density scaling exponent
γ	=	interfacial tension scaling exponent
σ	=	interfacial tension, m/t^2, mN/m

Superscript

s = liquid-vapor interface

Subscripts

c = critical point

I = constituent index

l = liquid phase

o = reference

v = vapor phase

REFERENCES

1. Guggenheim, E.A. and Adam, N.K.: "The Thermodynamics of Adsorption at the Surface of Solutions," *Proc. Roy. Soc.* (1933), **A139**, 218-236.
2. Cornelisse, P.M.W., Peters, C.J., and J. de Swaan Arons: "Application of the Peng-Robinson Equation of State to Calculate Interfacial Tensions and Profiles at Vapor- Liquid Interfaces," *Fluid Phase Equilibria* (1993), **82**, 119-129.
3. Macleod, D.B.: "On a Relation between Surface Tension and Density," *Trans. Faraday Soc.* (1923), **19**, 38-43.
4. Sugden, S.: "A Relation between Surface Tension, Density and Chemical Composition," *J. Chem. Soc.* (1924), **125**, 1177-1189.
5. Quayle, O.R.: "The Parachors of Organic Compounds," *Chem. Review* (1953), **53**, 439-586.
6. Weinaug, C.F. and Katz, D.L.: "Surface Tension of Methane-Propane Mixtures," *Ind. and Eng. Chemistry* (1943), **35**, No. 2, 239-246.
7. Katz, D.L., Mouroe, R.R., and Trainer, R.P.: "Surface Tension of Crude Oils Containing Dissolved Gases," *Petroleum Technology* (September 1943), 21-29.
8. Reno, G.J. and Katz, D.L.: "Surface Tension of n-Heptane and n-Butane containing Dissolved Nitrogen," *Industrial and Engineering Chemistry* (October 1943), **35**, No. 10, 1091-1093.
9. Hough, E.W. and Stegemeier, G.L.: "Correlation of Surface and Interfacial Tension of Light Hydrocarbons in the Critical Region," *Soc. Pet. Eng. J.* (December 1961), 259-263.
10. Lee, S.T. and Chien, M.C.H.: "A New Multiple Component Surface Tension Correlation Based on Scaling Theory," paper SPE/DOE 12643 presented at SPE/DOE 4th Symp. on EOR, Tulsa, OK, April 15-18, 1984.
11. Hugill, J.A. and Van Welsenes, A.J.: *Fluid Phase Equilibria* (1986), **29**, 383.
12. Firoozabadi, A., Katz, D.L., Soroosh, H., and Sajjadian, V.A.: "Surface Tension of Reservoir-Crude Oil/Gas Systems Recognizing the Asphalt in the Heavy Fraction," *SPERE*

(February 1988), 265-272.
13. Gasem, K.A.M., Dulcamara, P.B., Jr., Dickson, K.B., and Robinson, R.L., Jr.: "Test of Prediction Methods for Interfacial Tensions of CO_2 and Ethane in Hydrocarbon Solvents," *Fluid Phase Equilibria* (1989), **53**, 39-50.
14. Ali, J.K.: "Prediction of Parachors of Petroleum Cuts and Pseudocomponents," *Fluid Phase Equilibria* (1994), **95**, 383-398.
15. Fanchi, J.R.: "Calculation of Parachors for Compositional Simulation: An Update," *SPERE* (August 1990), 433-436.
16. Fawcett, M.J.: "Evaluation of Correlations and Parachors to Predict Low Interfacial Tension in Condensate Systems," paper SPE 28611 presented at the SPE 69th Annual Technical Conference and Exhibition, New Orleans, LA, September 26-28, 1994.
17. Guggenheim, E.A.: *Thermodynamics*, 3rd edition, North-Holland Publishing Company, Amsterdam (1957).
18. Guggenheim, E.A.: *J. Chem. Phys.* (1945), **13**, 253.
19. Stanley, E.H.: *Introduction to Phase Transitions and Critical Phenomena*, Oxford University Press, Oxford, U.K. (1982).
20. Fisher, M.E. and Scesney, P.E.: " Visibility of Critical-Exponent Renormalization," *Phys. Review A* (September 1970), **2**, 825-835.
21. Fisher, M.E.: *Phys. Review* (1968), 176, 257.
22. Sengers, J.M.H.L., and Sengers, J.V.: *How Close Is "Close to the Critical Point?"* North-Holland Publishing Company, Amsterdam (1981).
23. Rowlinson, J. and Widom, B.: *Molecular Theory of Capillarity*, Oxford University Press, Oxford, U.K. (1982).
24. Widom, B.: "Phase Equilibrium and Interfacial Structure," *Chemical Society Reviews* (1985), 121-139.
25. Moldover, M.R.: "Interfacial Tension of Fluids near Critical Points and Two Scale-factor Universality," *Phys. Review A* (1985), **31**, 1022-1033.
26. Haniff, M.D., and Pearce, A.J.: "Measuring Interfacial Tensions in a Gas Condensate System with a Laser-Light-Scattering Technique," *SPERE* (November 1990), 589-594.
27. Huygens, R.J.M., Ronde, H. and Hagoort, J.: "Interfacial Tension of Nitrogen and Volatile Oil Systems," paper SPE 26643 presented at the 68th SPE Annual Technical Conference and Exhibition, Houston, TX, October 3-6, 1993.
28. Wagner, O.R. and Leach, R.O.: "Effect of Interfacial Tension on Displacement Efficiency," *SPEJ* (December 1966), 335-344.
29. Firoozabadi, A. and Ramey, H.J., Jr.: "Surface Tension of Water-Hydrocarbon Systems at Reservoir Conditions," *JCPT* (May-June 1988), **27**, No.3, 41-48.
30. Satherley, J., Girault, H.H.J. and Schiffrin, D.J.: "The Measurement of Ultralow Interfacial Tension by Video Digital Techniques," *J. Colloid & Interface Science* (May 1990), **136**, No.2, 574-583.
31. Vargaftik, N.B.: *Tables on the Thermophysical Properties of Liquids and Gases*, John Wiley & Sons, Inc., 1975.
32. Greer, S.C.: "Coexistence Curves at Liquid-Liquid Critical Points: Ising Exponents and Extended Scaling," *Physical Review A* (1976) **14**, No.5, 1770-1780.

33. Satherley, J. and Schiffrin, D.: "The Measurement of Low IFT Values for Enhanced Oil Recovery," (August 1986), Progress Report to U.K. DOE, Winfrith.
34. Morrow, N.R., Chatzis, I. and Taber, J.J.: "Entrapment and Mobilization of Residual Oil in Bead Packs," *Soc. Pet. Eng. Res. Eng.* (1988) **3**, 927-935.
35. Cuiec, L.E., Bourbiaux, B. and Kalaydjian, F.: "Imbibition in Low-Permeability Porous Media: Understanding and Improvement of Oil Recovery," paper SPE 20259 presented at the 7th Annual Symposium on Enhanced Oil Recovery, Tulsa, OK, April 1990.
36. Hsu, J.C., Nagarajan, N. and Robinson, R.L., Jr.: "Equilibrium Phase Compositions, Phase Densities, and Interfacial Tension for CO_2 + Hydrocarbon Systems. 1. CO_2 + n-Butane," *J. Chem. Eng. Data* (1985), **30**, 485-491.
37. Nagarajan, N. and Robinson, R.L., Jr.: "Equilibrium Phase Compositions, Phase Densities, and Interfacial Tension for CO_2 + Hydrocarbon Systems. 2. CO_2 + n-Decane," *J. Chem. Eng. Data* (1986), **31**, 168-171.
38. Nagarajan, N. and Robinson, R.L., Jr.: "Equilibrium Phase Compositions, Phase Densities, and Interfacial Tension for CO_2 + Hydrocarbon Systems. 3. CO_2 + Cyclohexane. 4. CO_2 + Benzene," *J. Chem. Eng. Data* (1987), **32**, 369-371.
39. Gasem, K.A.M., Dickson, K.B., Dulcamara, P.B. Jr., Nagarajan, N. and Robinson, R.L., Jr.: "Equilibrium Phase Compositions, Phase Densities, and Interfacial Tension for CO_2 + Hydrocarbon Systems. 2. CO_2 + n-Tetradecane," *J. Chem. Eng. Data* (1989), **34**, 191-195.
40. Gasem, K.A.M., Dickson, K.B., Shaver, R.D. and Robinson, R.L., Jr.: "Experimental Phase Densities, and Interfacial Tension for CO_2 Synthetic-Oil and CO_2 Reservoir-Oil Systems," *SPERE* (1993) **8**, No. 3, 170-174.
41. Herz,W.: *Z. anorg. Chem.* (1927), **159**, 316.
42. Huygens, R.J.M., Ronde, H., and Hagoort, J.: "Interfacial Tension of Nitrogen/Volatile Oil Systems," paper SPE 26643 presented at the SPE 68th Annual Technical Conference and Exhibition, Houston, TX, October 3-6, 1993.
43. Pearson, T.G. and Robinson, P.L.: *J. Chem. Soc.* (1934), 736.
44. Rossini, F.D.: *Selected Values of Physical and Thermodynamic Properties of Hydrocarbons and Related Compounds*, Carnegie Press, Pittsburgh (1953).
45. Sage, B.H. and Lacey, W.N.: *Thermodynamic Properties of the Light Paraffin Hydrocarbons and Nitrogen,* API, New York (1950).
46. Katz, D.L.: *Bull. No. 114* (1949), The A&M College of Texas, 38.
47. Maass, O. and Wright, C.H.: *J. Am. Chem. Soc.* (1921), **43**, 1098.
48. Mumfod, S.A. and Phillips, J.W.C: *J. Chem. Soc.* (1928), 155.
49. Quayle, O.R., Day, A.R. and Brown, G.M: *J. Am. Chem. Soc.* (1944), **66**, 938.
50. Vogel, A.I.: *J. Chem. Soc.* (1946), 136.
51. Hunten, K.W. and Maass, O.: *J. Am. Chem. Soc.* (1929), **51**, 153.
52. Schenck, R. and Kintzinger, M.: *Rec. trav. Chem.* (1923), **42**, 759.
53. Godchot, M. and Cauquil, G.: *Compt. rend.*, 1931, Vol. 192, p. 1560.
54. Sugden, S.: *The Parachor and Valency,* George Routledge and Sons, Ltd., London, 1930.
55. Robinson, A.E.: Ph.D. Thesis, Emory University, 1950.
56. Vogel, A.I.: *J. Chem. Soc.* (1948), 1809.
57. Wibaut, J.P.: *Rec. Trav. Chim.* (1939), **58**, 375.

58. Wilson, R.C. and Henze, H.R.: *J. Am Chem. Soc.* (1941), **63**, 2112.
59. Manzoni-Ansidei, R.: *Boll. Sci. facolta chim.* (1940), ind. Univ. Bologna 4, 201.
60. Donaldson, R.E.: Ph.D. Thesis, Emory University, 1950.
61. Tuot, M.: *Comp. rend.* (1933), **179**, 1434.
62. Lee, F.H.: *J. Chinese Chem. Soc.* (1943), **10**, 16.
63. Ruzicka, L., Boekenoogen, H.A., and Edelman, H.J.: *Helv. Chim.*(1933), Acta 16, 487.
64. Sugden, S.: *J. Chem. Soc.* (1924), **125**, 1177.
65. Jeffery, G.H. and Vogel, A.I.: *J. Chem. Soc.* (1948), 654.
66. Truchet, R.: *J. Am. Chem. Soc.* (1931), **16**, 309.
67. Buehler, C.A., Gardner, T.S., and Robinson, P.L.: *J. Chem. Soc.* (1929), 1048.
68. Manzoni-Ansidei, R.: *Giorn. biol. ind. agrar. aliment* (1937), **7**, No. 5, 234.
69. Vogel, A.I.: *J. Chem. Soc.* (1948), 607.
70. Donaldson, R.E. and Quayle, O.R.: *J. Am. Chem. Soc.* (1950), **72**,
71. Bhatnagar, S.S. and Singh, B.: *J. chem. phys.* (1928), **25**, 21.
72. Hammick, D.L. and Wilmut, H.F.: *J. Chem. Soc.* (1935), 207.
73. Ahmed, T.I.: *Hydrocarbon Phase Behavior*, Gulf Publishing Co., Houston (1989), 64-65.
74. Simon, R., Rosman, A. and Zana, E.: "Phase-Behavior Properties of CO_2 -Reservoir Oil Systems," *SPEJ* (February 1978), 20-26.
75. Danesh, A., Dandekar, A., Todd, A.C. and Tehrani, D.H.: "Modified Scaling Law and Parachor Methods for Improved Prediction of Interfacial Tension," paper SPE 22710 presented at the 66th Annual Technical Conference and Exhibition of SPE in October 1991.
76. Fowler, R.H.: *Proc. Roy, Soc.* (London), 159 **A**, 229 (1937).
77. Ma, S.-K.: *Modern Theory of Critical Phenomena,* The Benjamin/Cummings Publishing Company, Inc., London (1976).

Table 3-1. Slopes of IFT vs $\Delta\rho$ data from Macleod.

Component Name	Reduced Temperature ($1-T/T_c$)	IFT (mN/m)	Slope
Ethyl Acetate	0.92–0.04	23.60–0.49	3.83
Ethyl Ether	0.90–0.07	16.49–0.64	3.94
Ethyl Alcohol	0.92–0.09	22.83–1.87	3.85
Phenol	0.72–0.06	20.28–0.99	3.84
Carbon Tetrachloride	0.93–0.12	25.68–1.93	3.91
Methyl Formate	0.91–0.07	24.62–0.87	3.90
Chlorobenzol	0.58–0.17	17.67–3.79	3.91
Acetic Acid	0.94–0.003	23.46–0.032	3.68

Table 3-2. Theoretical Values of the Critical Exponents.

Origin	β	γ	References
Van der Waal's Equation	0.5	1.5	
2-Dimensional Ising Model	0.125	1.75	[19] [77]
3-Dimensional Ising Model	0.312	1.25	[19] [77] [22]
Renormalization Group Theory	0.325	1.241	[22]
Currently Accepted Values	0.325	1.26	[23] [24] [25]

Table 3-3. Parachors of Petroleum Components.

Component	Parachor		Component	Parachor
Carbon Dioxide	82.00		Nitrogen	61.12
Hydrogen Sulphide	85.50		Methane	74.05
Ethane	112.91		Propane	154.03
n-Butane	193.90		n-Pentane	236.00
n-Hexane	276.71		n-Heptane	318.44
n-Octane	359.33		n-Nonane	399.57
n-Decane	440.69		n-Undecane	482.00
n-Dodecane	522.26		n-Tridecane	563.77
n-Tetradecane	606.05		n-Pentadecane	647.43
n-Hexadecane	688.50		n-Eicosane	853.67
n-Hexacosane	1108.90		n-Dotriacontane	1355.89
n-Hexacontane	2541.84		2-Methylbutane	234.87
2-Methylpentane	276.87		3-Methylpentane	273.84
2,2-Dimethylbutane	272.20		2,3-Dimethylbutane	272.12
2-Methylhexane	316.29		3-Methylhexane	314.76
3-Methylpentane	312.49		2,2-Dimethylpentane	314.83
2,3-Dimethylpentane	310.48		2,4-Dimethylpentane	315.36
3,3-Dimethylpentane	309.57		2,2,3-Trimethylbutane	309.45
2-Methylheptane	356.93		3-Methylheptane	355.57
4-Methylheptane	355.45		3-Ethylhexane	353.16
2,2-Dimethylhexane	353.92		2,3-Dimethylhexane	351.90
2,4-Dimethylhexane	353.29		2,5-Dimethylhexane	355.05
3,3-Dimethylhexane	351.10		3,4-Dimethylhexane	350.82
3-Ethyl-2-methylpentane	346.20		3-Ethyl-3-methylpentane	352.41

2,2,3-Trimethylpentane	348.24		2,2,4-Trimethylpentane	351.55
2,3,3-Trimethylpentane	347.13		2,3,4-Trimethylpentane	348.82
2,4-Dimethylheptane	390.10		2,5-Dimethylheptane	394.08
3,3-Dimethylheptane	385.71		2,2,3-Trimethylhexane	389.56
2,2,4-Trimethylhexane	390.49		2,2,5-Trimethylhexane	392.87
2,3,3-Trimethylhexane	387.38		2,3,5-Trimethylhexane	390.80
2,4,4-Trimethylhexane	388.85		3,3,4-Trimethylhexane	387.11
2,2,3,3-Tetramethylpentane	382.09		2,2,3,4-Tetramethylpentane	385.08
2,2,4,4-Tetramethylpentane	387.39		2,3,3,4-Tetramethylpentane	382.70
2,4-Dimethyloctane	433.20		2,7-Dimethyloctane	436.04
4,5-Dimethyloctane	429.00		2,4-Dimethyloctane	426.34
2,4,6-Trimethylheptane	433.00		2,4,7-Trimethyloctane	473.01
Cyclopentane	210.05		Cyclohexane	247.89
Methylcyclohexane	289.00		Ethylcyclohexane	328.74
1,1-Dimethylcyclohexane	326.22		cis-1,2-Dimethylcyclohexane	325.26
trans-1,2-Dimethylcyclohexane	328.26		1,2-Dimethylcyclohexane	327.09
cis-1,3-Dimethylcyclohexane	329.09		trans-1,3-Dimethylcyclohexane	326.69
1,3-Dimethylcyclohexane	329.02		cis-1,4-Dimethylcyclohexane	326.88
trans-1,4-Dimethylcyclohexane	330.20		1,4-Dimethylcyclohexane	328.99
n-Propylcyclohexane	369.52		Isopropylcyclohexane	366.16
1,1,3-trimethylcyclohexane	365.60		1,3,4-trimethylcyclohexane	364.93
n-Butylcyclohexane	410.51		Isobutylcyclohexane	407.71
sec-Butylcyclohexane	407.81		tert-Butylcyclohexane	404.73
Dicyclohexyl	460.41		Cycloheptane	285.24
Methylcycloheptane	325.19		Cyclooctane	322.56
Methylcyclooctane	362.33		2-Methylbicyclo[1,2,2]heptane	304.13

2-Methylbicyclo[2,2,2]octane	338.54		Decahydronaphthalene	381.58
trans-Decahydronaphthalene	379.41		cis-Decahydronaphthalene	375.32
Methylcyclopentadecane	638.23		Ethylene	101.53
Allylene	125.83		Propylene	143.02
2-Methyl-2-Butene	221.73		1-5-Hexadiene	254.35
3-Methyl-2-heptene	341.80		2,4-Dimethyl-4-hexene	338.55
2,5-Dimethyl-2-hexene	340.59		2,4-Dimethyl-4-heptene	381.98
2,5-Dimethyl-4-heptene	382.75		2,3,5-Trimethyl-2-hexene	379.41
2,4-Dimethyl-4-octene	422.05		2,4,6-Trimethyl-3-heptene	423.21
2,4,7-Trimethyl-4-octene	461.43		Acetylene	90.57
1-Octyne	335.26		3-Nonyne	373.10
3-Decyne	415.43		Phenylpropylacetylene	392.67
1-Undecyne	415.01		Butylpentylacetylene	456.59
Benzene	210.96		Toluene	252.33
Ethylbenzene	292.27		Indene	298.29
n-Propylbenzene	331.84		Isopropylbenzene	329.92
Naphthalene	321.01		n-Amylbenzene	412.32
n-Hexylbenzene	453.34		2-Amyl-1,4-dimethylbenzene	486.59
2-Hexyl-1,4-dimethylbenzene	527.97		2-Heptyl-1,4-dimethylbenzene	568.85
1,4-Dimethyl-2-octylbenzene	610.56		Triphenylmethane	602.29

Table 3-4. Correlation Coefficients of Hydrocarbon Parachors.

Hydrocarbons	*a*	*b*	SEOE
Normal Paraffins	2.97995377	18.17639160	4.617
Alkanes	2.98707461	11.73444748	5.884
Alkanes, Alkenes and Alkadienes	2.97924896	12.70571423	10.022
Alkanes, Alkenes, Alkadienes and Alkynes	2.97694945	11.37152950	12.594
Alkanes, Alkenes, Alkadienes, Alkynes and Cyclic Compounds	2.97649598	5.06389666	16.022
Alkanes, Alkenes, Alkadienes, Alkynes, Cyclic and Aromatic Compounds	2.95189214	3.71917152	21.941

SEOE = Standard Error Of Estimation.

Table 3-5 . Parachors of Oil Cuts.

Group	Parachor	Group	Parachor
C6	251.68	C7	287.10
C8	319.57	C9	360.90
C10	399.27	C11	437.65
C12	478.97	C13	520.30
C14	564.58	C15	611.81
C16	659.04	C17	703.32
C18	744.64	C19	780.07
C20	815.49	C21	862.72
C22	889.29	C23	924.7
C24	960.13	C25	998.51
C26	1033.93	C27	1066.40
C28	1101.82	C29	1131.34
C30	1166.76	C31	1196.28
C32	1228.75	C33	1261.23
C34	1293.70	C35	1317.31
C36	1349.78	C37	1373.40

C38	1405.87	C39	1432.43
C40	1464.91	C41	1485.57
C42	1515.09	C43	1541.66
C44	1571.17	C45	1594.79

Table 3-6 . Composition and Properties of Reservoir Fluids.

Component, mol%	System I	System II	System III	System IV	System V	System VI
CO2	2.98	1.00	2.02	0.16	0.01	0.01
N2	0.12	0.02	0.03	0.45	0.00	0.00
C1	66.87	36.13	51.53	36.71	31.00	31.30
C2	6.86	5.95	8.07	8.44	10.41	10.32
C3	3.95	4.44	5.04	6.03	11.87	10.68
i-C4	0.73	0.79	0.83	1.24	2.32	0.44
n-C4	1.82	2.12	2.04	3.67	5.00	6.30
i-C5	0.83	1.03	0.84	1.80	1.41	1.22
n-C5	1.03	1.25	1.05	2.36	3.00	2.77
C6	1.40	1.97	1.38	3.03	2.55	2.79
C7+	13.40	45.30	27.17	36.11	32.43	34.17
Total	100.00	100.00	100.00	100.00	100.00	100.00
C7+ molecular weight	164.7	227.4	217.0	234.3	199.0	190.3
C7+ specific gravity		0.870		0.868		0.833
Temperature, °F	73	180	180	170	130	130
Bubble point pressure, psia	5,901	2,155	4,589	2,573	1,666	

Table 3-7. Comparison of IFT Predictions with Measured Data.

Fluid Mixture	Pressure psia	Experiment IFT dyne/cm	Approach A	Predicted IFT, dyne/cm		
				B:	C:	D:
System I	2275	2.7	2.03	0.98	1.25	2.38
System II	185	19.5	11.80	10.68	11.43	16.05
	1150	10.1	7.30	5.13	5.74	9.83
	1650	6.7	5.50	3.14	3.61	7.35
	2150	5.5	4.05	1.79	2.12	5.36
System III	2315	4.6	3.23	1.58	1.90	4.20
	2815	3.3	2.23	0.87	1.08	2.88
	3315	2.3	1.47	0.45	0.57	1.89
	3815	1.3	0.90	0.21	0.28	1.16
System IV	1110	10.3	6.47	5.01	5.66	8.85
	1610	8.5	4.80	3.15	3.65	6.54
	2010	6.0	3.71	2.08	2.47	5.04
System V	2000	0.434	0.395	0.312	0.462	0.445
	2270	0.0583	0.0618	0.0437	0.0778	0.0606
Maximum Error, %		0	43.53	83.85	78.46	23.06
Average Error, %		0	28.43	58.21	51.87	11.01

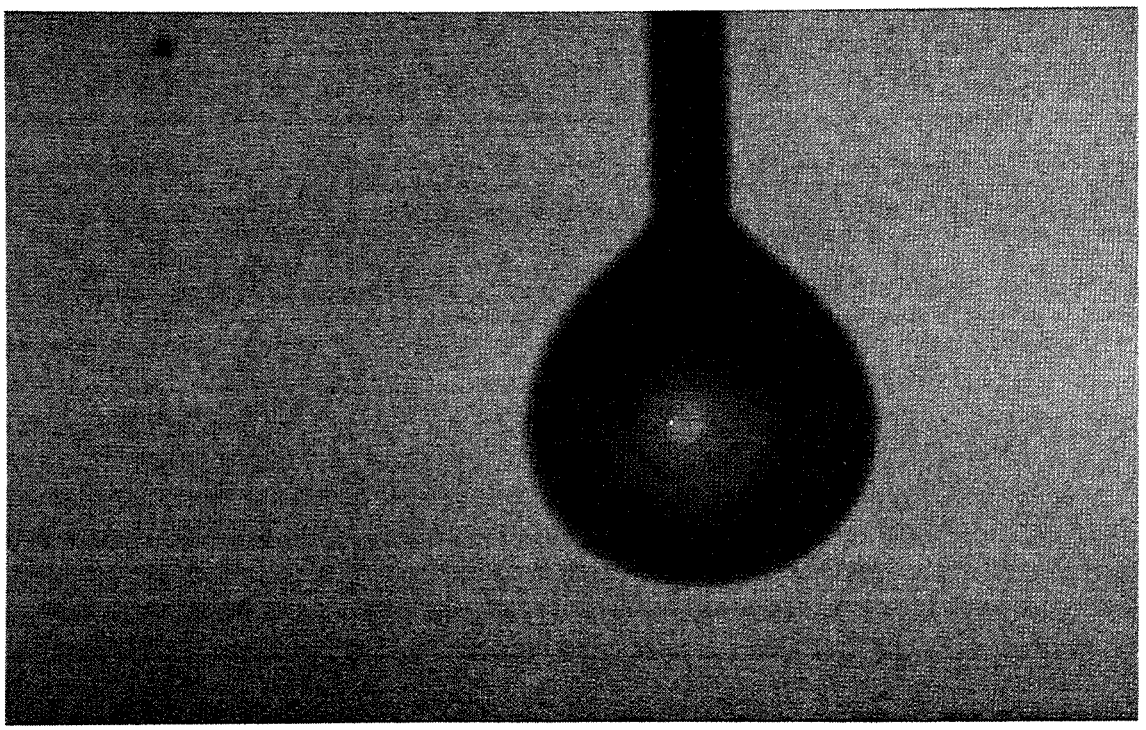

Fig. 3-1. Pendant drop for nitrogen/water system.

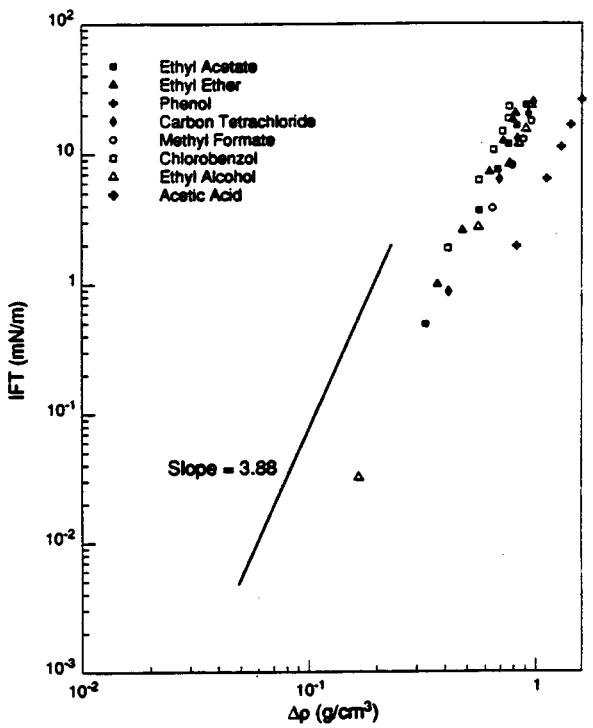

Fig. 3-2. Interfacial tension vs. density difference measurements by Macleod (also shown in Table 1). Theoretical slope of 3.88 is shown for comparison.

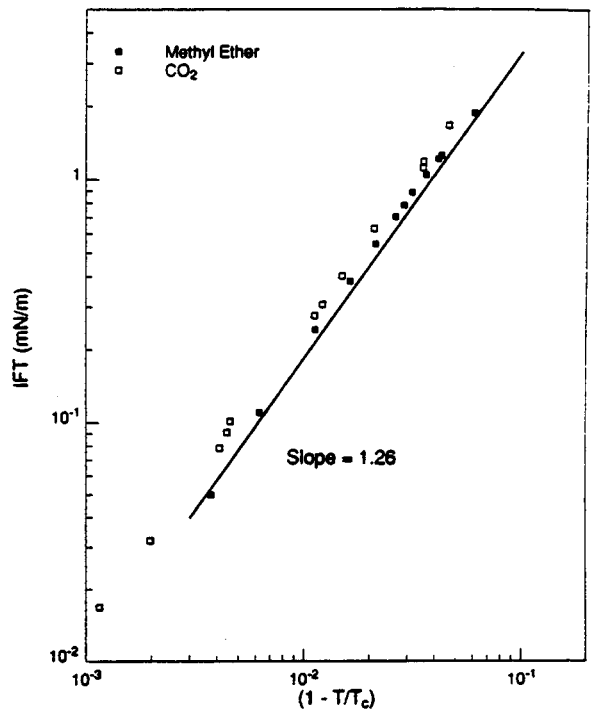

Fig. 3.3. Interfacial tension vs reduced temperature for methyl ether and CO_2. Theoretical slope of 1.26 is shown for comparison.

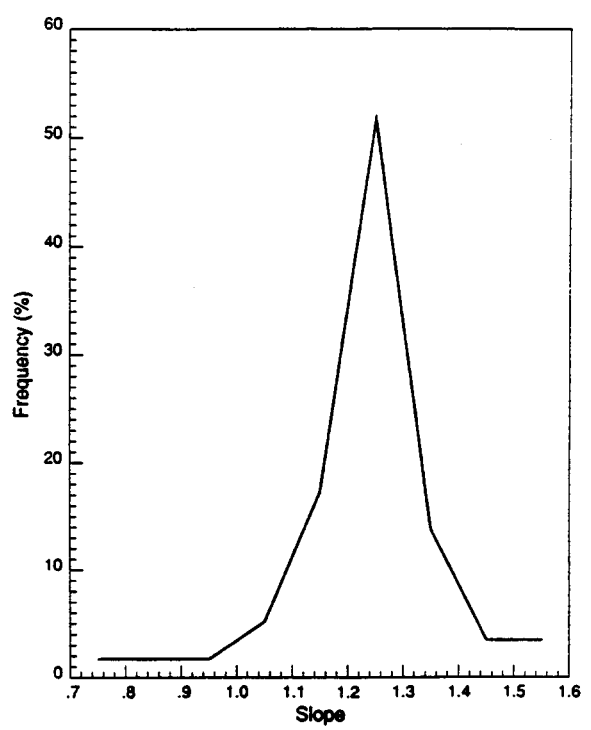

Fig. 3-4. Slope (γ in Eq. 6) distribution of IFT vs. $(1-T/T_c)$ plots for 57 pure components.

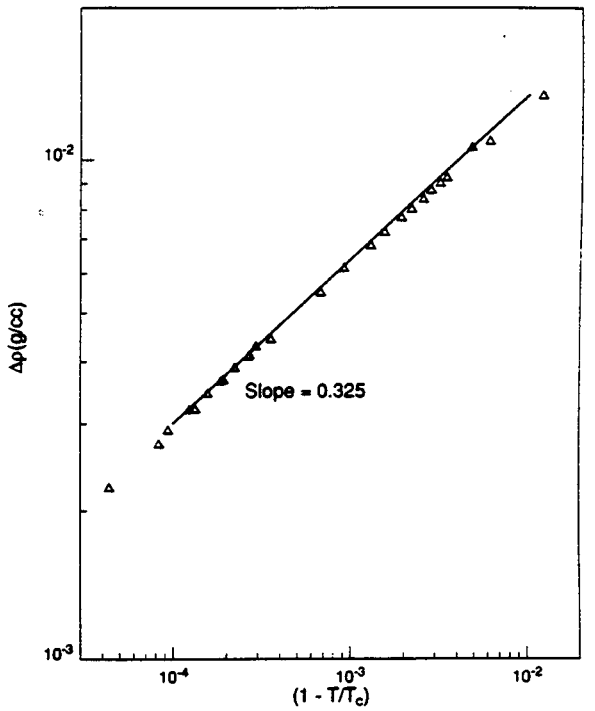

Fig. 3-5. Density difference vs reduced temperature for iso-butyric acid/water. Theoretical slope of 0.325 is shown for comparison.

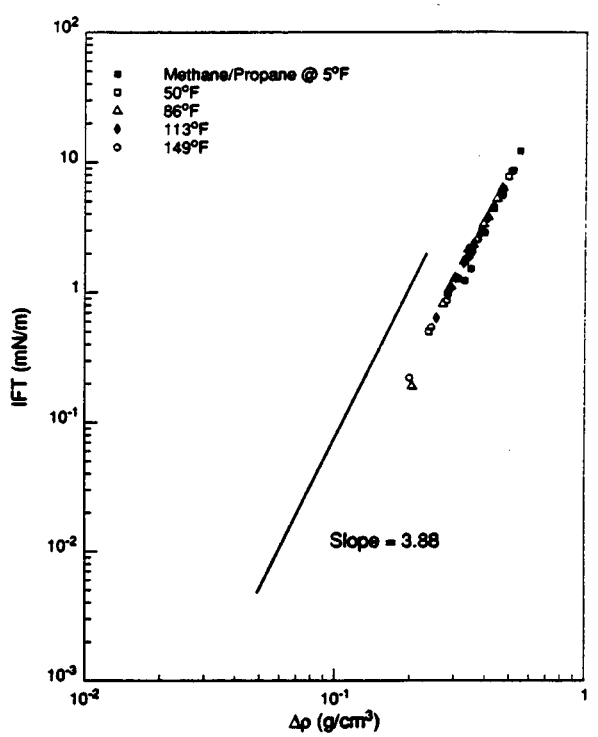

Fig. 3-6. Interfacial tension vs density difference for methane-propane mixtures. Theoretical slope of 3.88 is shown for comparison.

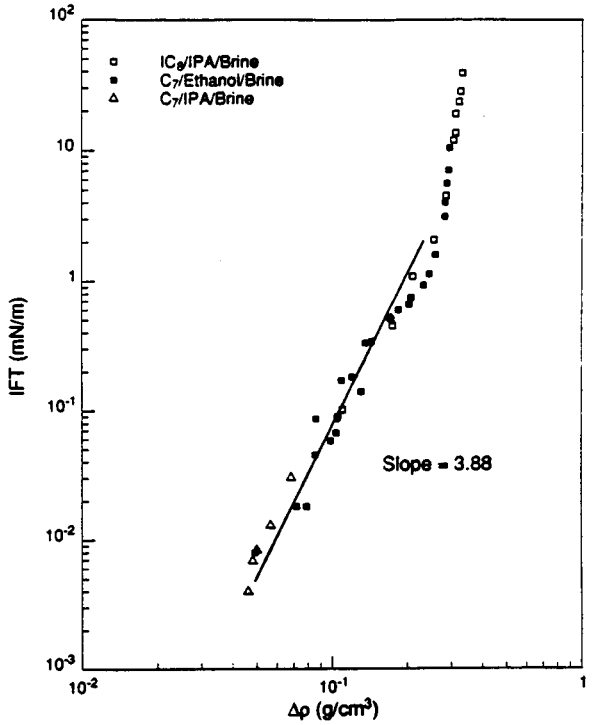

Fig. 3-7. Interfacial tension vs density difference for water/alcohol/oil systems. Theoretical slope of 3.88 is shown for comparison.

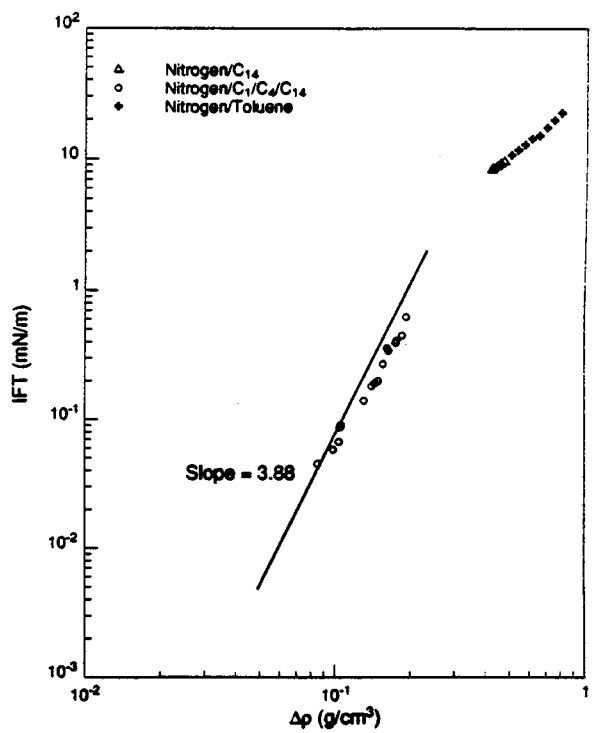

Fig. 3-8. Interfacial tension vs density difference for N_2/oil systems. Theoretical slope of 3.88 is shown for comparison

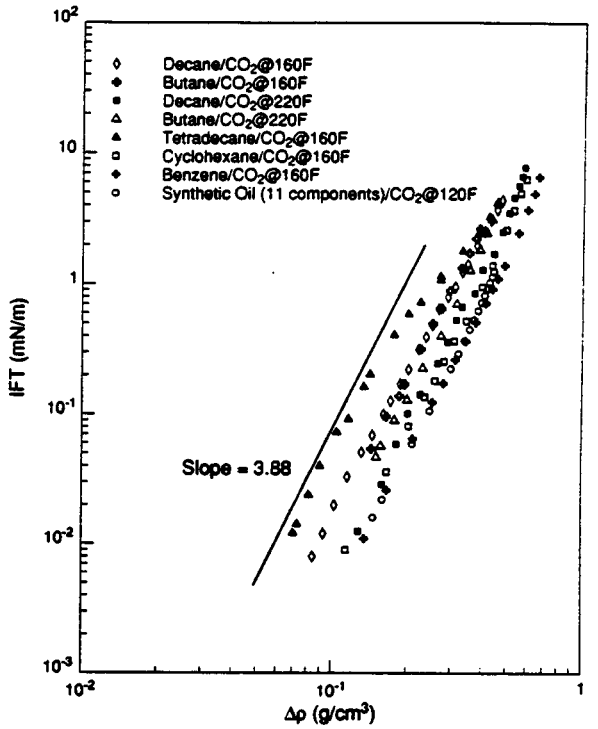

Fig. 3-9. Interfacial tension vs density difference for oil/CO_2 systems. Theoretical slope of 3.88 is shown for comparison.

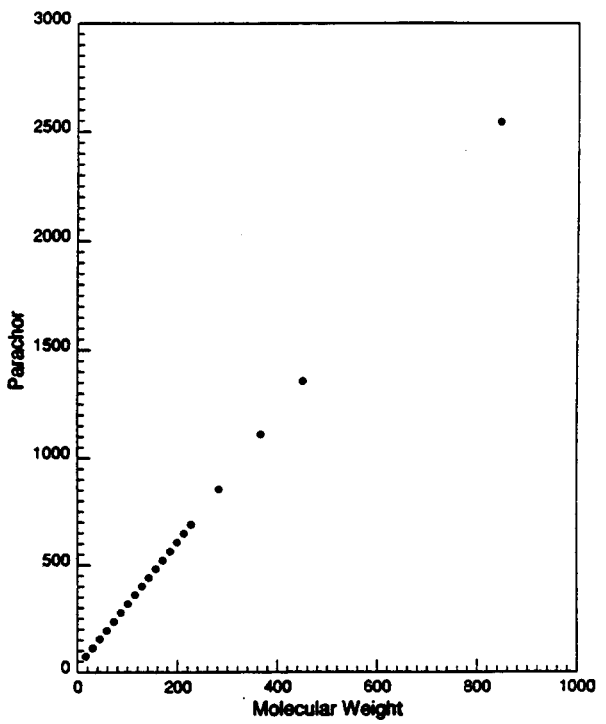

Fig. 3-10. Parachor vs molecular weight for 20 normal paraffins.

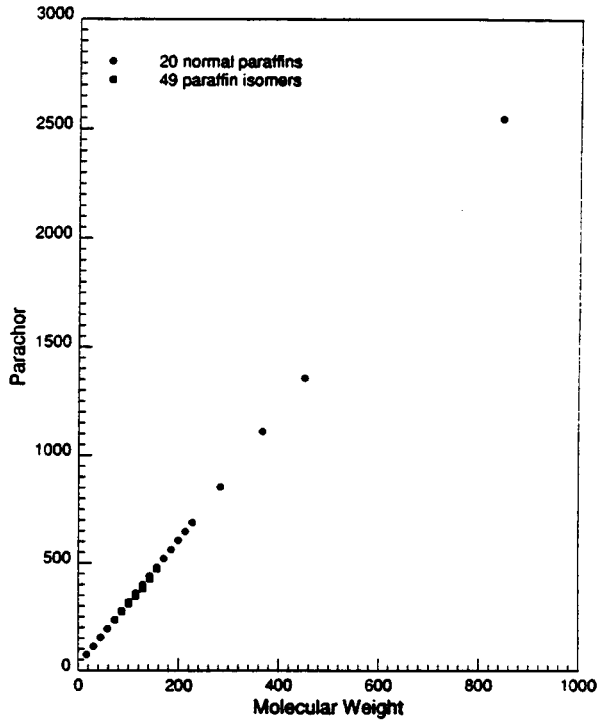

Fig. 3-11. Parachor vs. molecular weight for 69 hydrocarbons.

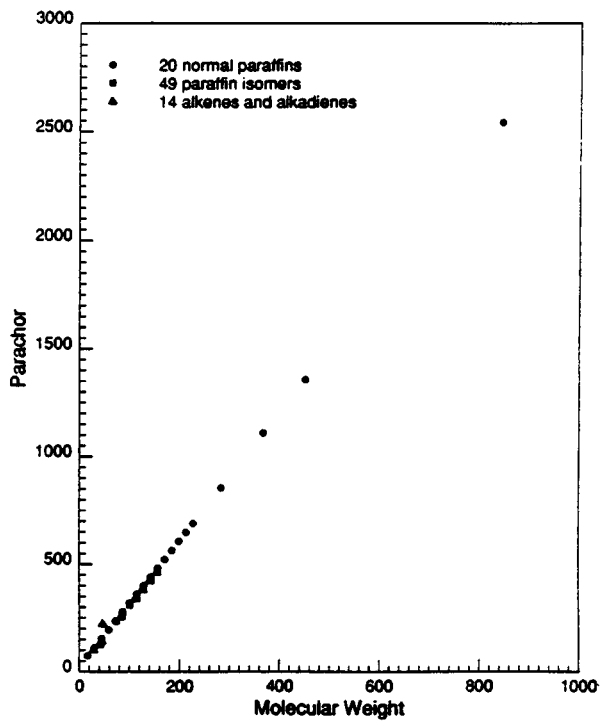

Fig. 3-12. Parachor vs molecular weight for 83 hydrocarbons.

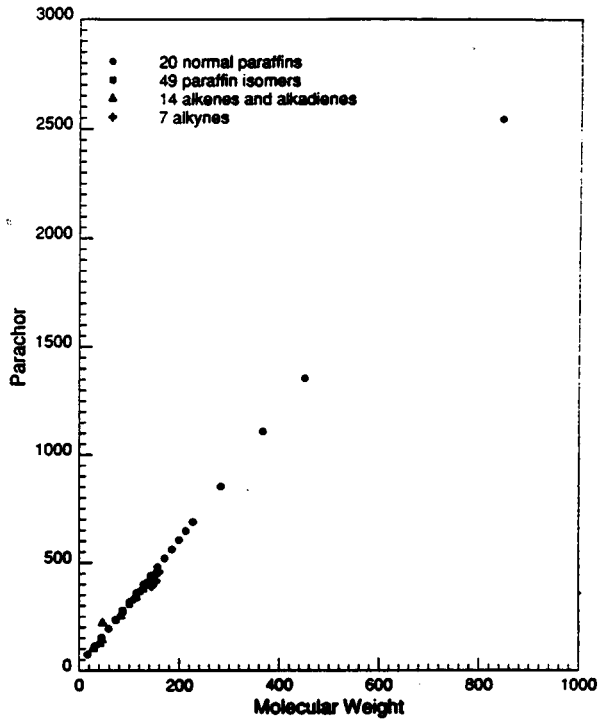

Fig. 3-13. Parachor vs molecular weight for 90 hydrocarbons.

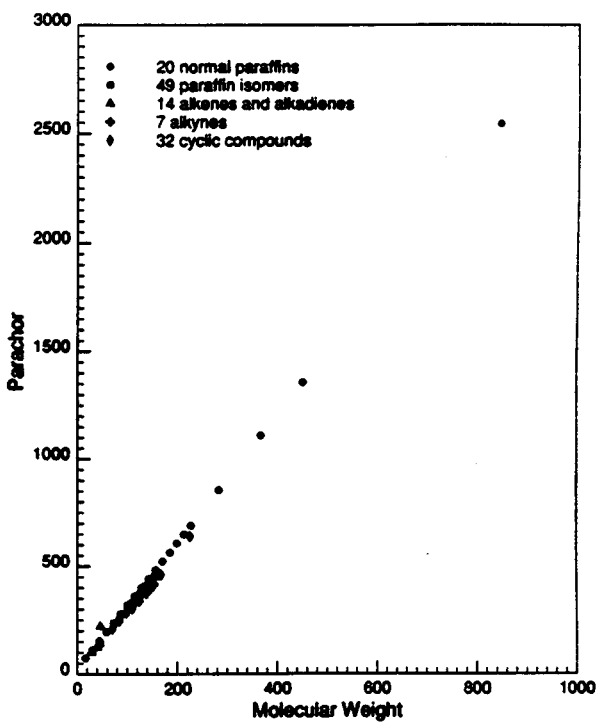

Fig. 3-14. Parachor vs molecular weight for 122 hydrocarbons.

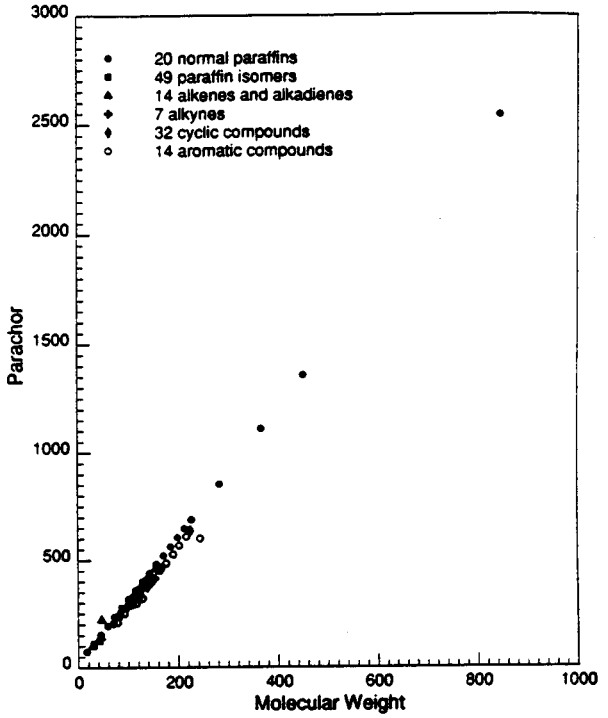

Fig. 3-15. Parachor vs molecular weight for 136 hydrocarbons.

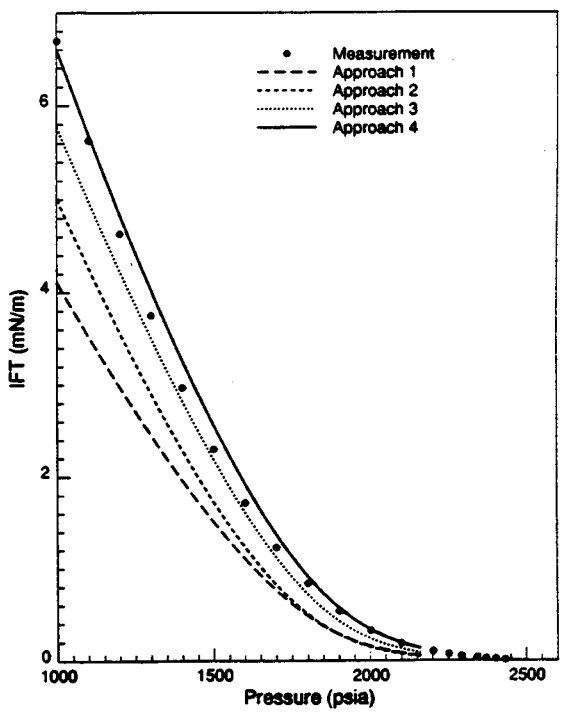

Fig. 3-16. Measured and PREOS-predicted IFT of system VI.

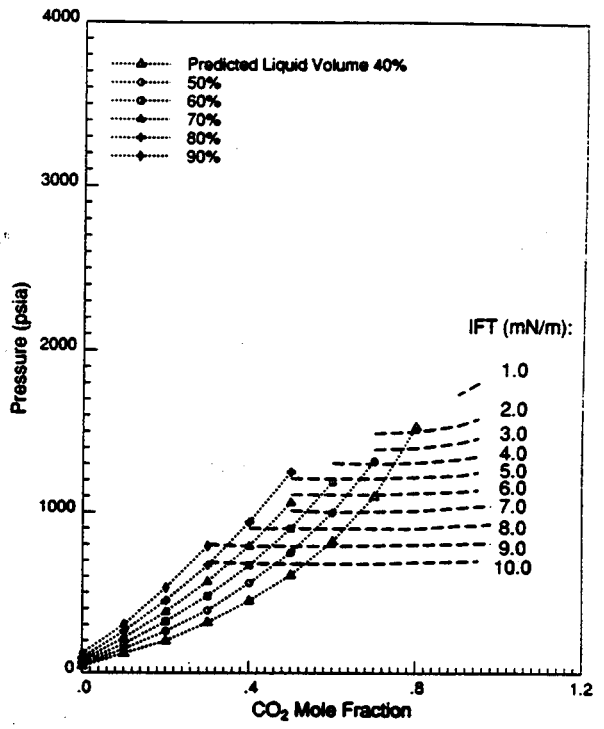

Fig. 3-17. PREOS-predicted IFT of CO_2/Spraberry separator oil.

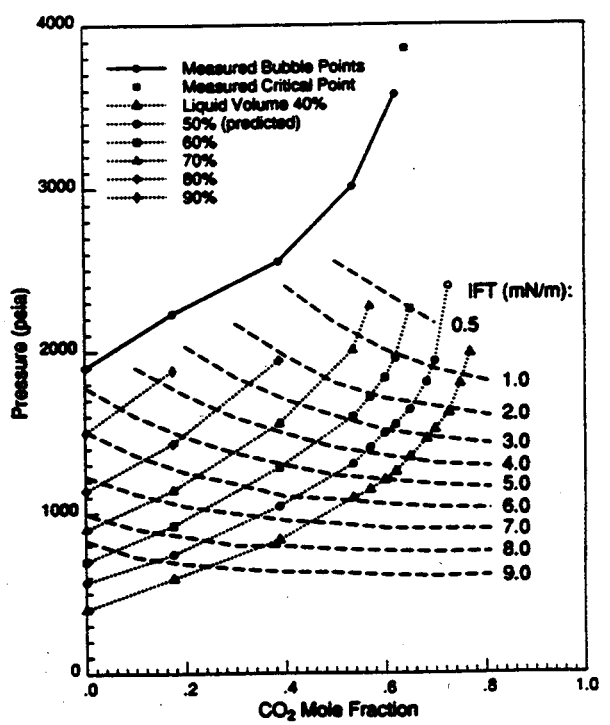

Fig. 3-18. PREOS-predicted IFT of CO_2/Sprabery reservoir oil.

CONCLUDING REMARKS

This first annual technical report on PRRC's current CO_2 project defines three specific tasks, and describes the work that has been performed on them to date. Each of the three tasks is directed towards solving a particular problem encountered in CO_2 flooding, the solutions to which will make possible more efficient oil recovery from fields which are amenable to production enhancement by high-pressure CO_2 injection, especially heterogeneous reservoirs.

The report is divided into three sections, each of which covers in detail the work performed on the corresponding task. In each case, vital introductory material is covered, as well as technical descriptions of progress that is of importance to the domestic oil industry. The results of this project will be directly implemented into ongoing and planned field work.

ACKNOWLEDGMENTS

It is a pleasure to acknowledge financial assistance from the U.S. Department of Energy and the State of New Mexico. Support has also come from several oil companies—although as is well known, they themselves are operating under greatly reduced research budgets. The following companies are supporting the PRRC's research into CO_2 applications: AMOCO Production Company, The Chevron Chemical Company, Marathon Oil Company, Mobil E & P, USA, Mobil Research and Development Corporation, Parker & Parsley Development Company, and Texaco E & P Technology Department.

In addition to the Principal Investigators, mention must be made of the numerous other individuals who have participated actively in the research work. These include Drs. Jyun-Syung Tsau, S-H. (Eric) Chang, and Boyun Guo, as well as other laboratory workers Amulya Dixit, T-C. Huang, and Hossein Yaghoobi. Invaluable technical assistance has also been rendered by Jim McLemore, John Kernodle, David Fritchman, and Robert Svec. Also, thanks to Liz Bustamante, who put this document together.

☆U.S. GOVERNMENT PRINTING OFFICE: 1995 - 660-029/20065